

KfK 4686
Juni 1990

The Karlsruhe Cosmic Ray Project KASCADE

P. Doll, J. Engler, P. Gabriel, M. Gettert, H. J. Gils, A. Hanser,
D. Heck, N. Heide, H. Keim, H. O. Klages, J. Knapp,
W. Kriegleder, H. J. Mathes, H. J. Mayer, H. Müller,
J. Oehlschläger, H. Rebel, G. Schatz, H. Schieler,
G. Schmalz, T. Thouw, G. Völker, S. Zagromski, B. Zeitnitz
Institut für Kernphysik

Kernforschungszentrum Karlsruhe

KERNFORSCHUNGSZENTRUM KARLSRUHE

Institut für Kernphysik

KfK 4686

THE KARLSRUHE COSMIC RAY PROJECT KASCADE

P. Doll, J. Engler, P. Gabriel, M. Gettert, H.J. Gils, A. Hanser, D. Heck, N. Heide,
H. Keim, H.O. Klages, J. Knapp, W. Kriegleder, H.J. Mathes, H.J. Mayer,
H. Müller, J. Oehlschläger, H. Rebel, G. Schatz, H. Schieler, G. Schmalz,
T. Thouw, G. Völker, S. Zagromski, B. Zeitnitz

Kernforschungszentrum Karlsruhe GmbH, Karlsruhe

Als Manuskript gedruckt
Für diesen Bericht behalten wir uns alle Rechte vor

Kernforschungszentrum Karlsruhe GmbH
Postfach 3640, 7500 Karlsruhe 1

ISSN 0303-4003

Abstract

KASCADE (KARlsruhe Shower Core Array DEtector) is an extensive air shower experiment being under construction at the Kernforschungszentrum Karlsruhe (49°N, 8°E, 110 m a.s.l.). The main aim is to obtain information on the primary composition of cosmic rays at energies above 3×10^{14} eV. In this energy range a remarkable change of slope of the energy spectrum is observed. Results at lower energies seem to indicate that this is correlated with a change of the chemical composition. Besides other valuable informations the proof of such an effect would have important consequences for our understanding of the origin of cosmic rays. The basic approach of KASCADE is to measure a large number of parameters for each individual shower. These include electron and muon numbers, the lateral distributions as well as number, energy, and spatial distribution of hadrons in the shower core. Extensive Monte Carlo simulations of air showers are discussed using a specially developed code for hadronic interactions. These simulations of air shower development and of detector response lead to an experiment layout which is described in detail. The arrangement will also be able to identify point sources in the quoted energy range.

DAS KARLSRUHER HÖHENSTRAHLUNGS - PROJEKT KASCADE

KASCADE (KARlsruhe Shower Core Array DETector) ist ein Experiment zur Beobachtung ausgedehnter Luftschauer, das zur Zeit im Kernforschungszentrum Karlsruhe (49°N, 8°E, 110 m a.s.l.) aufgebaut wird. Das Hauptziel sind Informationen über die primäre Element-Zusammensetzung der kosmischen Strahlung bei Energien über $3 \cdot 10^{14}$ eV. In diesem Energiebereich wird eine bemerkenswerte Änderung im Abfall des Energiespektrums beobachtet. Ergebnisse bei tieferen Energien scheinen anzudeuten, daß dies mit einer Veränderung der chemischen Zusammensetzung einhergeht. Neben anderen wertvollen Informationen würde der Beweis eines solchen Effektes wichtige Konsequenzen für unser Verständnis über den Ursprung der kosmischen Strahlung haben.

Das KASCADE-Experiment zielt darauf ab, eine große Anzahl von Parametern jedes einzelnen Schauers zu bestimmen. Diese Parameter sind die Gesamtzahl und lateralen Verteilungen der Elektronen und Myonen, sowie die Zahl, Energie und räumliche Verteilung der Hadronen im Schauerkerneln. Ausgiebige Monte-Carlo Simulationen mit einem speziell entwickelten Rechenprogramm für die hadronischen Wechselwirkungen werden diskutiert. Die Ergebnisse dieser Simulationen für die Entwicklung der Luftschauer-Kaskaden sowie für die Detektor-Ansprehwahrscheinlichkeit führen zu dem beschriebenen Aufbau der KASCADE Anordnung, die auch in der Lage ist, Punktquellen im angegebenen Energiebereich zu identifizieren.

1. Introduction

The nature of the cosmic ray composition is a crucial issue for determining the origins and sources of cosmic rays. However, the experimental information for the energy range above 10^{14} eV is still rather scarce and controversial. The flux is so low that direct measurements in balloon or satellite experiments appear to be impossible. The traditional technique is to detect extensive air showers produced by the primary cosmic ray particles in the atmosphere. Photons, protons or heavier nuclei interact with the nitrogen and oxygen nuclei and generate an extensive shower, composed of different components of secondary particles. Such an air shower is a widely spread pancake of particles moving through the atmosphere with nearly the speed of light for many kilometres.

KASCADE (KARlsruhe Shower Core and Array DETector) is an experiment being under construction at Kernforschungszentrum Karlsruhe (49° N, 8° E, 110 m a.s.l.) in order to study air showers induced by high energy particles above $3 \cdot 10^{14}$ eV. The main objective is to obtain information on the chemical compo-

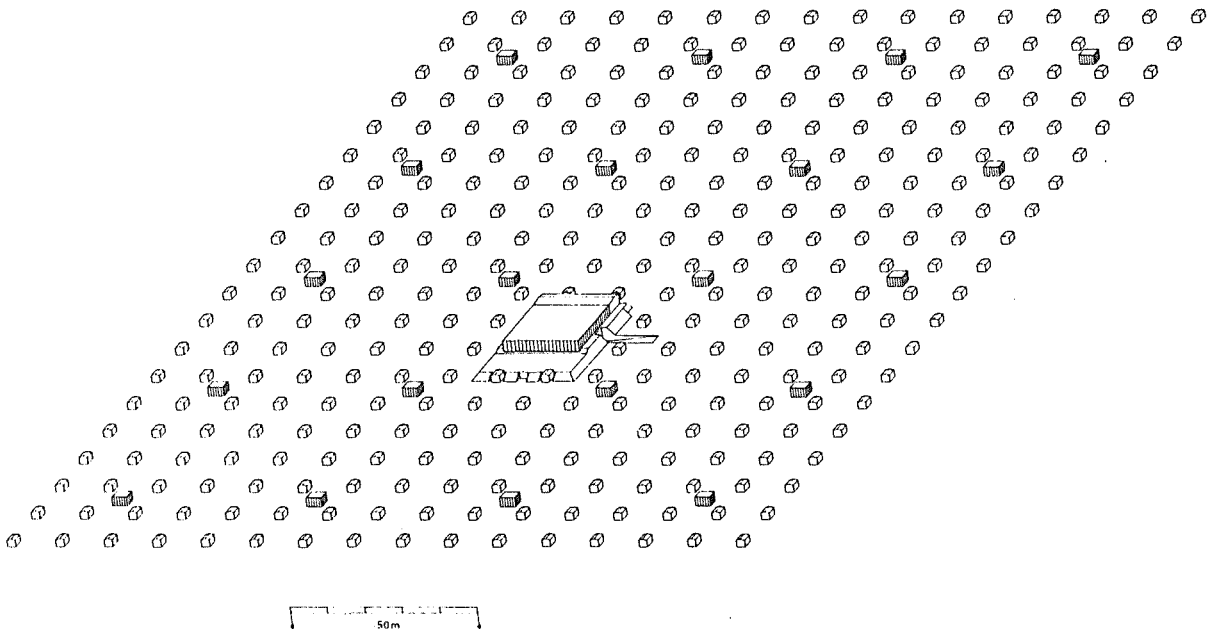


Fig. 1.1 Schematic view of the "KARlsruhe Shower Core and Array DETector"
(KASCADE)

sition of cosmic rays. In the considered energy range a remarkable change in the slope of the energy spectrum is observed. Results at lower energies indicate that this change may be due to a change of the chemical composition. In addition, the arrangement will be able to identify point sources in the quoted energy range.

Tab. 1.1 Some characteristic features of the KASCADE set-up.

I. Array

Size	50 000 m ²
Detectors for the electromagnetic component (EM)	1264
Muon detectors	316
Energy threshold (EM)	3 MeV
Energy threshold (μ)	300 MeV
Rates $E_0 \geq 10^{14}$ eV	2 s ⁻¹
$E_0 \geq 10^{16}$ eV	20 h ⁻¹
Angular resolution	
$E_0 \geq 5 \cdot 10^{14}$ eV	< 0.4°

II. Central detector

Size	16 x 20 m ²
Dynamic energy range	10 GeV - 10 TeV
Energy resolution	35%
Position resolution	25 cm
Energy threshold for muons	2 GeV
Position resolution for muons	6 mm

The basic approach of KASCADE is to measure a large number of characteristic parameters for each individual shower. These include electron and muon numbers, the lateral distributions of the electromagnetic and muon components as well as the number, energy and spatial distribution of hadrons in the shower core. Fig. 1.1 displays schematically the detector field. The main components (tab. 1.1) are an array in an area of 200 x 250 m² size with 316 array detector stations of > 3 m² active area for measuring both the electrons and muons. Hadrons and muons are detected in a central calorimeter of 16 x 20 m² size and a total depths of 11 interaction lengths containing 9 active detector layers.

The layout is based on extensive Monte Carlo simulations of the air shower development in the atmosphere and of the detector response. From the results of the simulation calculations it is expected that mass values differing by a factor of 4 can be discriminated experimentally. This implies that the three most abundant groups of primary particles, protons plus alpha particles, the CNO group and the iron group can be distinguished.

The following report describes in detail the scientific aims of the experiment, the ingredients and results of the air shower simulations, and discusses the experimental and technical aspects which lead to the layout of KASCADE presented here.

2. Scientific objectives

The main objective of the experiment is to obtain information about the chemical composition of the primary cosmic ray particles in the energy range above a few 10^{14} eV. As will be shown in the following sections this requires the measurement of a larger number of parameters of each individual extensive air shower. As a consequence, the KASCADE experiment will obtain much more detailed information about the properties of extensive air showers than previous experiments and hence will contribute to a number of other open questions in extensive air shower research.

2.1 Chemical composition

Although cosmic rays are known for more than 75 years [1] their origin is still an open question in a considerable range of primary energies. Most primary particles are positively charged, as can be deduced from their deflection in the magnetic field of the earth. The identification of hadrons (quite a number of which have been discovered in cosmic ray experiments) in the cascades induced by the primary particles in the atmosphere indicates that most primaries are also hadrons. Since charged particles are deflected by magnetic fields in interstellar space their direction of incidence into the atmosphere does no more contain any information about their origin. Therefore their energy distribution and their chemical nature are the only quantities measurable on earth which can give us hints about their origin and their fate on their way from source to solar system.

The most direct way to identify the chemical nature of a cosmic ray primary is by measurements above the atmosphere of the earth before the particles have interacted with air nuclei. Such measurements have been performed from high flying balloons and satellites over the last few decades and have yielded results up to energies of a few tens of TeV. The main results of these measurements can be summarized as follows [2 - 5]:

1. The overall composition is very similar to the mean composition of the solar system or the local interstellar medium with the following exceptions.

2. Hydrogen and helium are less abundant in cosmic rays by factors of 10 and 3 at low energies, respectively, but this depletion diminishes with increasing energy [4].
3. There is a correlation between the cosmic ray abundance and the first ionization potential such that elements with high ionization energy are slightly depleted. The reason for this correlation is not understood [4].
4. The elements Li, Be, B, F and Sc to Mn which are comparatively rare in the solar system are much more abundant in cosmic rays, but their abundance decreases faster than average with increasing energy. This is attributed to their production by spallation reactions of the more abundant elements C, O and Fe.
5. The abundance of Fe in cosmic rays decreases less fast with increasing energy than the total intensity. While at low energies there is approximately 10 times more O than Fe in the primary radiation these two elements are equally abundant near 1 TeV [6].

Measurements above the atmosphere give the most direct information about the chemical nature of the primaries, but they are limited in energy due to the steep decline of intensity with energy because detectors on satellites and balloons are limited in weight and hence in size. It is not to be expected that such measurements will be extended by more than a factor of ten beyond the results available today [7], i. e. to more than several hundreds of TeV for iron nuclei and several tens of TeV for protons. (This dependence on the primary mass results from the fact that the detectors employed measure essentially the velocity or the energy per nucleon of the particles, hence the limit is roughly proportional to the mass number.) Beyond this limit only ground based measurements are possible.

On the other hand, the question of the primary chemical composition above a few hundred TeV is of special interest for the following reasons:

- The primary spectrum of cosmic ray particles follows power laws for more than three decades below 1 PeV and above 10 PeV (cf. fig. 2.1). In between, a change of slope occurs whose origin is unknown. It might be an indication of different acceleration mechanisms prevailing in the different energy regions. This then could be reflected by a change of composition.
- During the last 10 years considerable progress has been made in understanding the acceleration mechanism. According to the presently accepted theory the bulk of the cosmic ray particles is accelerated by shock waves produced by supernovae in the interstellar medium [8,9]. This

mechanism works well up to energies of a few hundred TeV [10]. Recently a modification of this theory has been proposed which would allow acceleration up to ca. 10 PeV or beyond [11]. This modified theory would imply that the higher energy particles do not originate in the average interstellar medium but rather in the surface of giant stars shortly before their explosion as a supernova. Hence a different chemical composition would be expected.

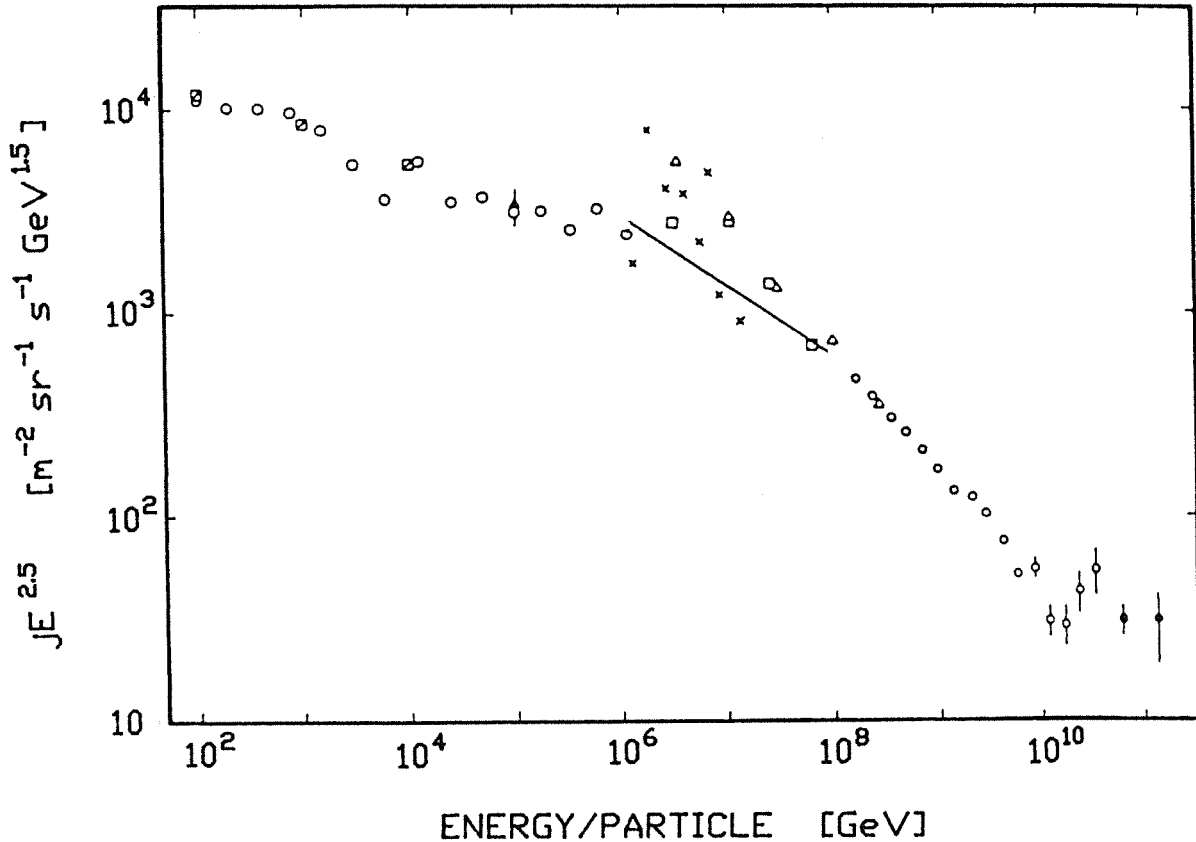


Fig. 2.1 Differential energy spectrum of the primary cosmic rays between 10^2 and 10^{11} GeV. The data points are from Linsley [12], the short straight line around 10^7 GeV represent preliminary results of the HEGRA experiment [13].

- The charged cosmic ray particles are confined to the galactic plane by interstellar magnetic fields. They probably leak out of the Galaxy at irregularities of these fields. Since the gyromagnetic radius of a relativistic particle is proportional to its energy and inversely proportional to its charge one expects the leakage of protons to start at lower energy than that of heavier nuclei. If the composition at the source is independent of energy the cosmic rays should become depleted in protons and alpha particles at the point where the leakage starts. A determination of this energy would thus give information about the magnetic confinement of cosmic rays to the Galaxy which is unknown at present.

Measurements from the ground suffer from the severe disadvantage that only the remnants of the particle cascade which develops in the atmosphere of the earth can be observed. The thickness of the atmosphere corresponds to ca. 12 nuclear interaction lengths and to ca. 28 radiation lengths. So it is by no means obvious to what extent the observables depend on the chemical nature of the primary. This question is discussed in detail in the next section and it is shown that measurable differences between showers initiated by complex nuclei or single nucleons of the same energy remain.

The problem of the chemical composition of cosmic ray primaries in the energy range of extensive air showers, i. e. above 10^{14} eV, is by no means new. The proceedings of the International Cosmic Ray Conferences (the last of which were held at Bangalore 1983, La Jolla 1985, and Moscow 1987) contain a considerable number of contributions which try to answer this question, and a detailed review has been given by Watson [56]. The results are very contradictory, though. In our opinion, these discrepancies are due to the following facts:

- In an extensive air shower experiment, the particles which can be observed represent the tenth or later generation of successive interactions in the cascade. Therefore, their type, numbers, energies, and directions depend on the properties of the interactions between the shower particles and air nuclei. It is consequently well known that different assumptions about the strong interaction model may lead to completely different conclusions concerning the chemical composition (cf. [14], e. g.).
- All observables in an extensive air shower exhibit strong fluctuations. For most previous experiments the detector areas employed were so small that the fluctuations of at least the muon and hadron numbers were governed by sampling rather than by the intrinsic shower properties. This implies that only mean shower characteristics could be determined, averaged, e. g., over the unknown chemical composition. (As far as the muon number is concerned, the CASA experiment [15] under construction at Dugway, Utah, is a notable exception.) The KASCADE experiment will have a large sensitive area such that the fluctuations of the measured quantities will not be notably influenced by sampling (except possibly near threshold). In addition, it attempts to measure a large number of parameters of each individual shower. The latter fact is important because it should allow an independent check of the interaction model.

2.2 Point sources

Several years ago a group of the Kiel University reported an excess of cosmic ray events in the PeV range centred on the X-ray source Cygnus X-3 and showing a temporal modulation with the well known X-ray period [16]. These events have to be attributed to neutral particles since charged ones would be deflected by the interstellar magnetic fields and hence not retain their directional information. The natural explanation would be PeV gamma rays emitted by Cygnus X-3 because neutrons would decay on their way between source and earth and the interaction cross section of neutrinos is too small to account for the observed events. An enigmatic feature of the observation is, though, that the muon contents of the showers is comparable to that of the average (i. e. hadronic) event [17] whereas a gamma shower should have a muon content smaller by about an order of magnitude [18]. This discovery has triggered considerable activity all around the world. At present about a dozen experiments are in operation, construction or in the planning stage to study this phenomenon and to search for further sources of this kind. Despite a considerable effort over the last few years the results are scarce although a number of confirming (albeit partly conflicting) observations has been reported [19-23]. It is clear from various experiments, though, that the flux as observed by the Kiel group cannot be constant in time, but must be subject to considerable fluctuations. Especially the high muon content of the showers which cannot be explained with our present understanding of elementary particle physics has aroused interest and speculation.

The KASCADE detector system, although designed primarily for investigating cosmic ray composition, will be one of the largest assemblies for the study of cosmic ray point sources. Due to its location near sea level the energy threshold will be around 300 TeV and therefore inferior to detectors at mountain altitude [15, 24 - 26] but it will cover the energy range of the original Kiel experiment. Its large sensitive area for electrons and muons will make it competitive in the higher energy region with most dedicated experiments presently in operation or under construction. Details of the performance of KASCADE in this field will be given in section 4.

2.3 Further objectives

A number of observations concerning extensive air showers are reported which do not appear to find an easy explanation on the basis of our present knowledge of high energy interactions. None of these seem to be generally accepted, but they may give hints to new phenomena in particle physics or astrophysics.

The KASCADE experiment will register a large number of parameters of each individual shower and give more detailed information about shower properties than previous experiments. There is therefore a high probability that such phenomena, if real, will show up in our planned measurements. A few of these subjects will be briefly discussed in the following paragraphs.

The Tien Shan group has operated a hadron calorimeter of 36 m² at a site 3300 m above sea level (690 g/cm²). They report the observation of events with particles which penetrate deeper into the calorimeter than expected of any known ones. This phenomenon has been called the *Tien Shan Effect* [27, 28]. The "long flying component" in the calorimeter exhibits an attenuation length which reaches values above 1000 g/cm² in lead for hadrons of 100 TeV entering the calorimeter. The difference in atmospheric depth between the Tien Shan and the Karlsruhe sites (ca. 330 g/cm²) is much smaller than the thickness of the Tien Shan calorimeter. So any such unknown particle, if sufficiently longlived, has a chance to reach the KASCADE calorimeter. The flux of high energy hadrons at sea level is, of course, considerably smaller than at mountain altitude. This is compensated at least partly by the much larger size of our calorimeter.

For a number of extensive air shower experiments the observation of *delayed particles*, especially hadrons and muons, has been reported [28 - 30]. These observations have been explained by longlived hadrons which differ from any particles observed in accelerator experiments. It is obvious that the central calorimeter of the KASCADE experiment with its fast timing capability should be able to identify such particles if they exist.

A group of the University of Leeds have measured the distribution of electrons in the shower core by spark chambers of 35 m² size. They observed a flattening of the electron distribution within a few meters from the shower axis at an energy near 1 PeV [31] (*"core flattening"*). A similar effect is observed at mountain altitude [32]. Simulation calculations based on conventional high energy physics are unable to reproduce this feature [32].

The KASCADE detector system has a very large area of muon detectors such that the fluctuation of the number of observed muons will be governed by the intrinsic fluctuation of extensive air showers rather than by the sampling statistics. If a low number of muons is indeed typical for extensive air showers induced by gamma rays, as predicted by the present theory of electromagnetic interaction, our experiment should be well suited to identify *diffuse gamma rays*, i. e. gamma rays which do not originate in pointlike objects. Such a gamma radiation has been observed in the MeV to GeV region [33, 34]. It is attributed to the decay of neutral

pions produced by cosmic rays in the interstellar medium and hence allows to trace the cosmic rays over a large portion of the Galaxy [35]. It is interesting to check this explanation at the much higher energies accessible to the KASCADE experiment. The Tien Shan group have argued, based on the measurements with their hadron calorimeter, that it is not sufficient to rely on a small muon number alone for identifying gamma induced showers but that the absence or near-absence of hadrons in the shower is needed as an additional condition [36]. Again the large hadron calorimeter planned for the KASCADE experiment would offer excellent capability for such a discrimination.

3. Air shower simulations

3.1 Qualitative considerations

A number of quantities observable in extensive air showers are reported in literature to depend on the atomic number of the primary cosmic ray particle. These include the ratio of electron and muon numbers [18], the energy of hadrons [37], and the lateral distribution of hadrons in the shower core [38]. This can be understood qualitatively on the basis of the energy dependence of the high energy nucleon-nucleon interaction which has recently been reviewed by Geich-Gimbel [39]. An incident nucleus with mass number A and energy E may, in first approximation, be considered as the superposition of A independent nucleons of energy E/A because the binding energy of the nucleus is very small as compared to the total energy for the cases of interest. It is well known from experiment that the average number of secondary particles in a high energy nucleon-nucleon interaction exhibits approximately a logarithmic increase with energy. Hence A nucleons of energy E/A produce more secondary particles than one nucleon of energy E . Since most secondaries are pions a fraction of which decay into muons it is not surprising that the average muon number is larger in a shower induced by a nucleus than in one induced by a proton of equal energy. The inelasticity of the interaction, i. e. the mean energy loss of the primary in the collision, is almost independent of energy. Therefore the secondaries in a proton induced shower have, in general, higher energy, hence the higher energy of hadrons at observation level. The differences in lateral distribution result from the fact that the mean transverse momentum of secondaries changes only very slowly with primary energy.

All these qualitative statements have, of course, to be checked by calculations. This was done by extensive simulations with a newly developed program called CORSIKA (COsmic Ray SIMulations for KASCADE). This program is briefly

outlined in the next subsection. A detailed description of the program will be published.

3.2 Outline of the CORSIKA program

The Monte Carlo program CORSIKA was composed of three existing programs describing different parts of the simulation of extensive air showers. In addition to the changes necessary for combining these programs a number of modifications and refinements have been incorporated in CORSIKA. These will be described in the following paragraphs.

3.2.1 Strong interactions at high energy

Strong interaction above 10 GeV center-of-mass energy are calculated with a program developed by J. N. Capdevielle [40]. It uses a parametrization of experimental data based on the dual parton model. The basic philosophy of the approach has been published [6], so only a short description is given here.

For each collision, first it is determined by a random choice whether the interaction was diffractive. If not, the multiplicity is chosen randomly based on the negative binomial distribution with parameters derived from experimental data [39,41]. For each secondary particle its type and transverse momentum are selected taking into account the dependence of the mean transverse momentum on particle type and energy. Then the rapidity is determined. Its distribution is described by a superposition of three Gaussians, two of which account for the fragmentation of the two hadrons and the third one for the influence of the residual nucleus [41,42]. Thereby energy and direction of the secondary particles are determined. The residual energy is attributed to the last particle. If it turns out to be negative the event is discarded and the Monte Carlo generator is started anew from the beginning. Capdevielle has shown that this procedure describes the experimental distributions of secondary particles very well [41].

In the case of a diffractive interaction the excitation energy of the nucleon is determined assuming a cross section inversely proportional to the square of the mass of the excited system. The decay of the excited nucleon is then treated in exactly the same way as a non-diffractive interaction of the same total energy [41].

In air showers particles collide with nuclei rather than with free nucleons. This does not only modify the total and inelastic cross sections but probably also influences particle production. In the energy range relevant for KASCADE no experimental information on nucleon-nucleus collisions is available but measurements at lower energy indicate that the incident nucleon may interact

successively with more than one nucleon of the target nucleus. The theoretical analysis of low energy data has shown that in such cases diffractive interactions are suppressed [43]. Therefore the following procedure was adopted: The probability of n ($n \leq A$) successive collisions of the incident hadron in the same nucleus was calculated treating the target nucleus as an extended object with the nucleon distribution taken from experiment [44,45]. Here it was assumed that the inelastic cross section is not modified by the preceding interactions. For $n = 1$ particle production was calculated according to a free nucleon-nucleon interaction as described above. For $n > 1$ only non diffractive particle production was assumed.

If the incident cosmic ray particle is a complex nucleus frequently more than one of the incident nucleons will interact during a collision with an air nucleus. The probability of m nucleons interacting is calculated with a simple geometrical model which is based on the empirical nucleon distributions of the two colliding nuclei [44,45] and employs the adequate averaging over the impact parameter. The non interacting nucleons proceed as free particles at the original energy/nucleon.

3.2.2 Strong interactions at low energy

Strong interactions below 10 GeV center-of-mass energy are calculated by a program developed by P. K. F. Grieder [46]. This program also provided the overall architecture of the CORSIKA program. It is based on the isobar model and describes the empirical cross sections up to ISR energies very well. It has been used previously for extensive air shower simulations [37, 47].

3.2.3 Electromagnetic interactions

CORSIKA contains two different options for treating the electromagnetic interactions in the simulated showers.

The *NKG option* uses the analytical formula of Nishimura, Kamata and Greisen [48] to calculate the longitudinal development of the electromagnetic subcascades for each individual gamma ray or electron produced by particle decay. The lateral electron distribution at observation level is calculated by a modified version of the NKG formula since it is well known that the original formula does not describe the distribution at large distances precisely [49]. The contributions of the individual gamma rays or electrons are then summed up. Most of the simulations for the design of the KASCADE experiment have been performed with this version because the required computing time is smaller by a factor of 15 than with the EGS option.

The *EGS option* of CORSIKA performs a full Monte Carlo simulation of all strong *and* electromagnetic interactions employing the EGS4 program [50] widely used in high energy physics. A number of modifications were introduced in order to speed up the program for this specific application. The height dependence of air density was introduced using a parametrization due to Linsley which is very similar to the US standard atmosphere* ; the density dependent Sternheimer correction [51] was incorporated; the photoproduction of pions and muons was included; following a proposal by Spitzer [52] photons and electrons of comparatively low energy produced at high altitude above observation level are discarded employing a cut depending on height and energy (typically 2 % of the electromagnetic particles at observation level are lost this way).

3.3 Results of the simulation with CORSIKA

3.3.1 What was simulated ?

As described above KASCADE will be able to measure the number of electrons falling inside an area of around 200 x 250 m² with a sampling of around 2 %. Hadrons reaching the central calorimeter can be recognized above the threshold of 10 GeV and their energy can be measured with an accuracy of ≈ 35 %. The number of muons inside the array can be measured by the array stations and the μ -chambers below the calorimeter with a sampling of around 3 %. The analysis of the simulated air-showers was performed on the basis of such a detector.

For the first analysis altogether 2700 showers have been generated (most of them with vertical incidence), using the analytic treatment of the electromagnetic component with the NKG-formulas.

- p initiated showers were chosen to represent the group of light primaries. The difference between p and He was found to be smaller than the fluctuations of p showers, hence no distinction can be made on our level of precision.
- O initiated showers were simulated to represent the C, N, O group of primaries observed in cosmic rays.
- Fe initiated showers finally were simulated as an example of the group of heavy nuclei.

The elements between He and the CNO group, and between the CNO and the Fe group amount to only a few percent of the total flux of cosmic rays [5, 6].

*We thank Dr. A.M. Hillas for making the formulae available to us.

The primary energies were varied between $2.5 \cdot 10^{14}$ and $2.8 \cdot 10^{15}$ eV, which is just below the knee in the differential energy spectrum of the cosmic ray flux and just above the lower threshold of KASCADE.

3.3.2 Dependence of shower properties on the primary energy and particle

As mentioned in sect. 3.1 an incident nucleus will generate more secondary hadrons, but at a lower mean energy than a primary proton.

But this surplus in the number of particles has to compete with the lower fraction of particles penetrating the thick atmosphere to reach the detector. For our experiment the absorption effect is still dominating but with increasing energy the copious production of secondaries gains more importance.

3.3.2.1 Hadrons

We obtain flatter distributions for the hadrons and a lower hadron density in the center of Fe showers than in p showers. In fig. 3.1 the particle density ρ_h of hadrons with energies ≥ 10 GeV is plotted for different primaries at $E_0 = 10^{15}$ eV as a function of the core distance r . The difference in the central density is one order of magnitude.

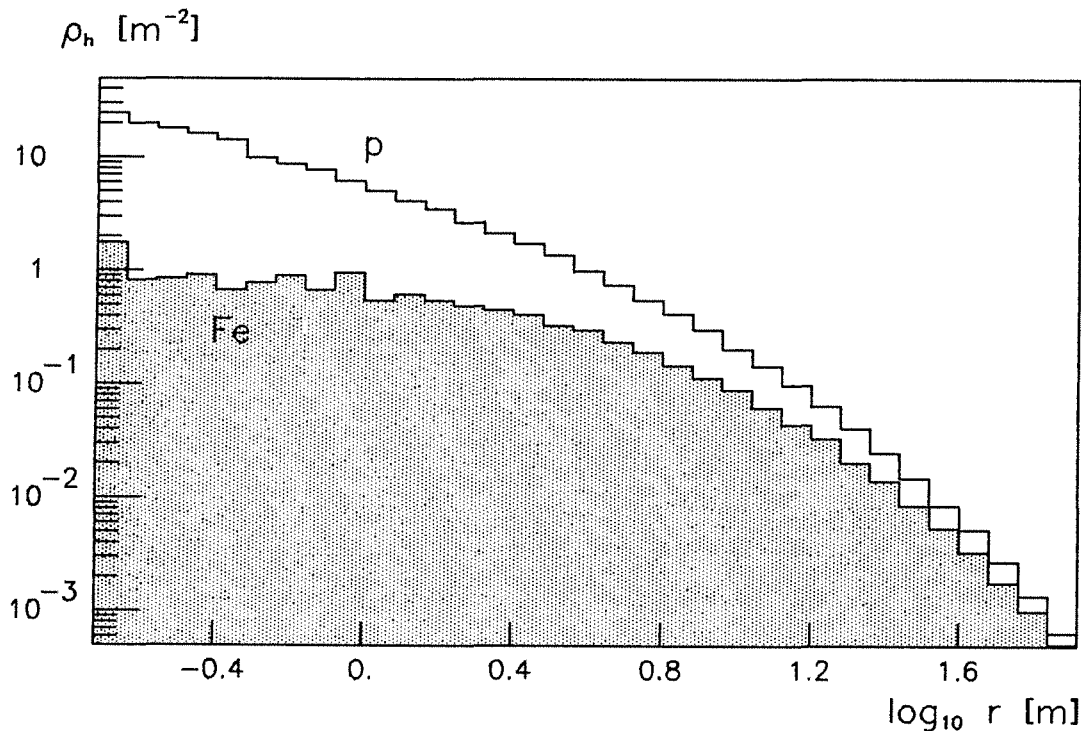


Fig.3.1 Mean particle density for hadrons ≥ 10 GeV versus the core distance r ($E_0 = 10^{15}$ eV).

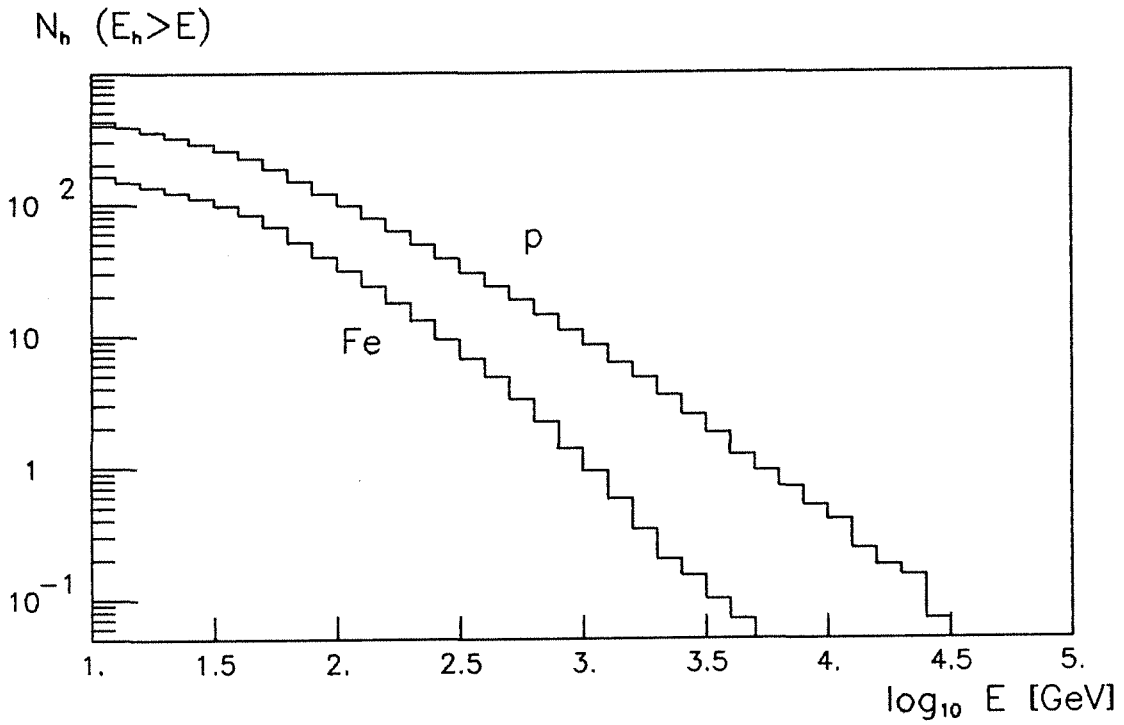


Fig.3.2 Average energy spectrum of hadrons in showers of $E_0 = 10^{15}$ eV originating from different primaries.

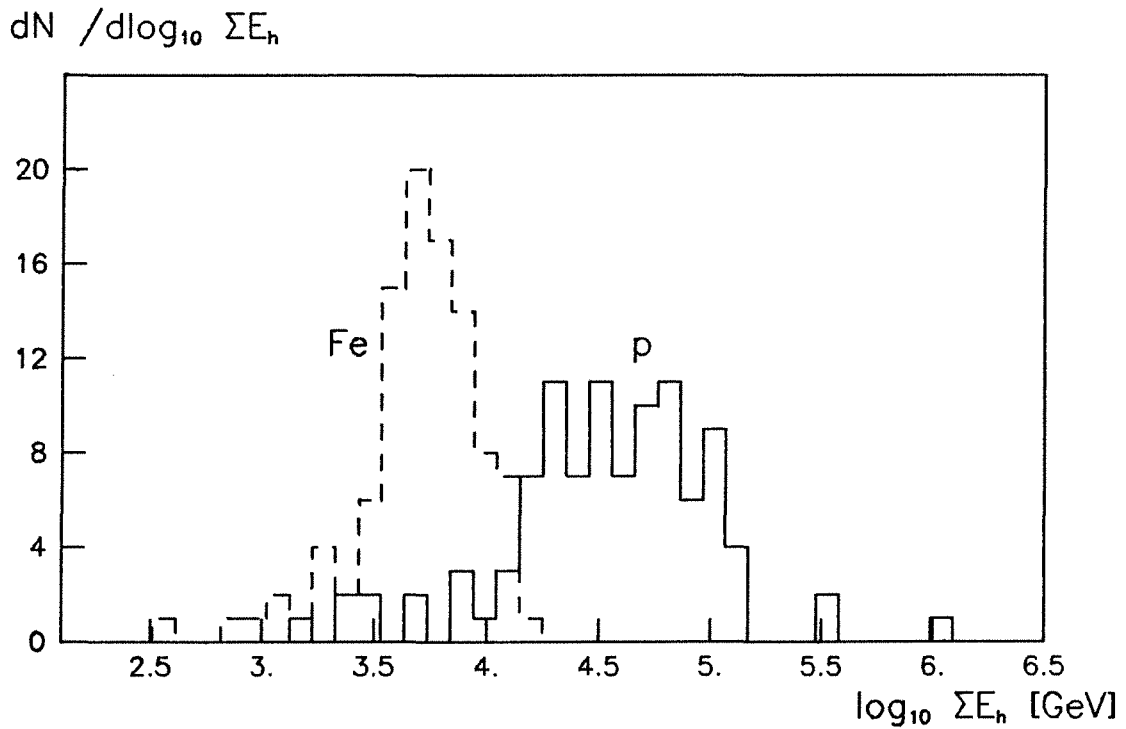


Fig.3.3 Distribution of the energy sum ΣE_h of hadrons with $E_h \geq 10$ GeV and $r \leq 5$ m for showers of $E_0 = 10^{15}$ eV originating from different primaries.

p showers contain on average hadrons with higher energies than Fe showers, because their initial energy / nucleon is higher. This can be seen in fig. 3.2, showing the energy spectra of the hadrons originating from p and Fe showers at 10^{15} eV. The hadrons get up to 1 % of the initial proton energy and only around 1 ‰ of the initial Fe energy.

As will be shown in sect. 5.5 we can distinguish single hadrons up to densities of 3 hadrons / m^2 . For higher energies one gets dense cores where only an energy measurement will be possible and no single hadrons can be identified.

The energy sum, however, provides an equally good possibility to separate p and Fe showers because it combines the number of hadrons and the mean energy of hadrons, both being higher for p induced showers than for Fe showers at the same primary energy. In fig. 3.3 the energy sum of all hadrons above 10 GeV within a core distance $r \leq 5$ m is shown for p and Fe induced showers of a primary energy of 10^{15} eV.

3.3.2.2 Muons

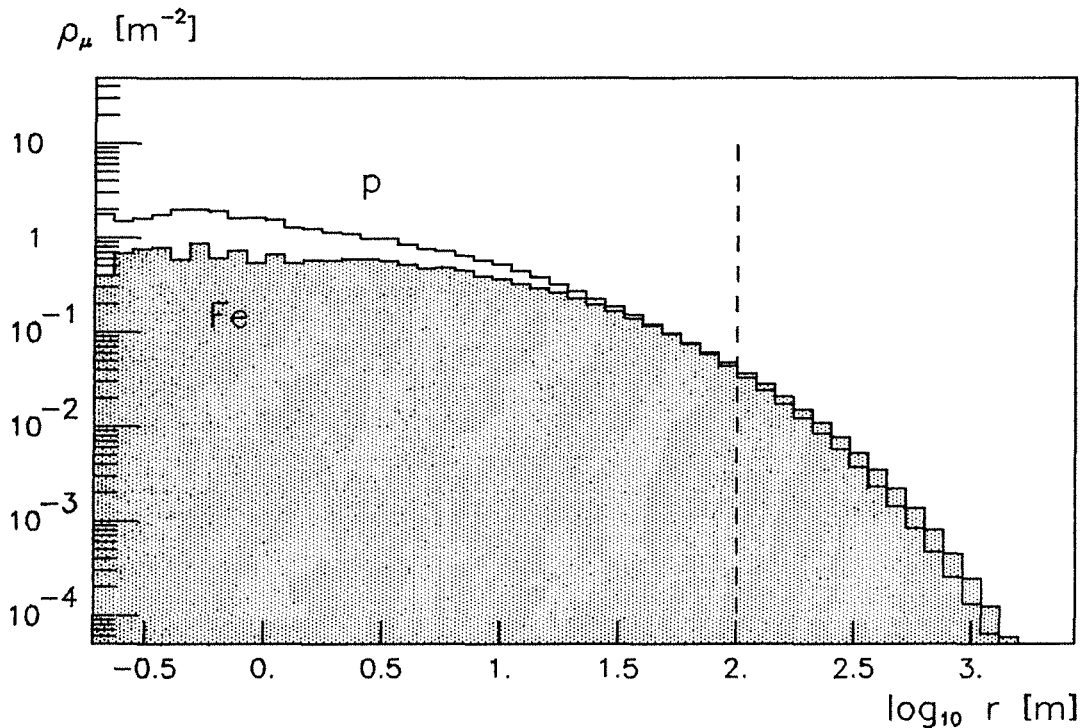


Fig. 3.4 Mean particle density ρ_μ of muons in showers of $E_0 = 10^{15}$ eV created by different primaries.

The μ component originates from decaying pions over the complete length of the shower. Muons reach the observation level at high probability before they react

with matter or decay. Their number is therefore correlated with the number of secondaries produced in total. As for hadrons we get a flatter lateral distribution of muons in Fe showers than in p showers. This can be seen in fig. 3.4. For iron-induced showers we get more muons than for p showers as expected.

The broadening of the lateral distribution with increasing A compensates the increase in the number of muons to some extent if one regards the number inside a certain area. By chance the effects cancel for a detector area of $200 \times 250 \text{ m}^2$ and the number of muons falling in the array N_μ^a is almost independent of the type of primary particle at a fixed primary energy.

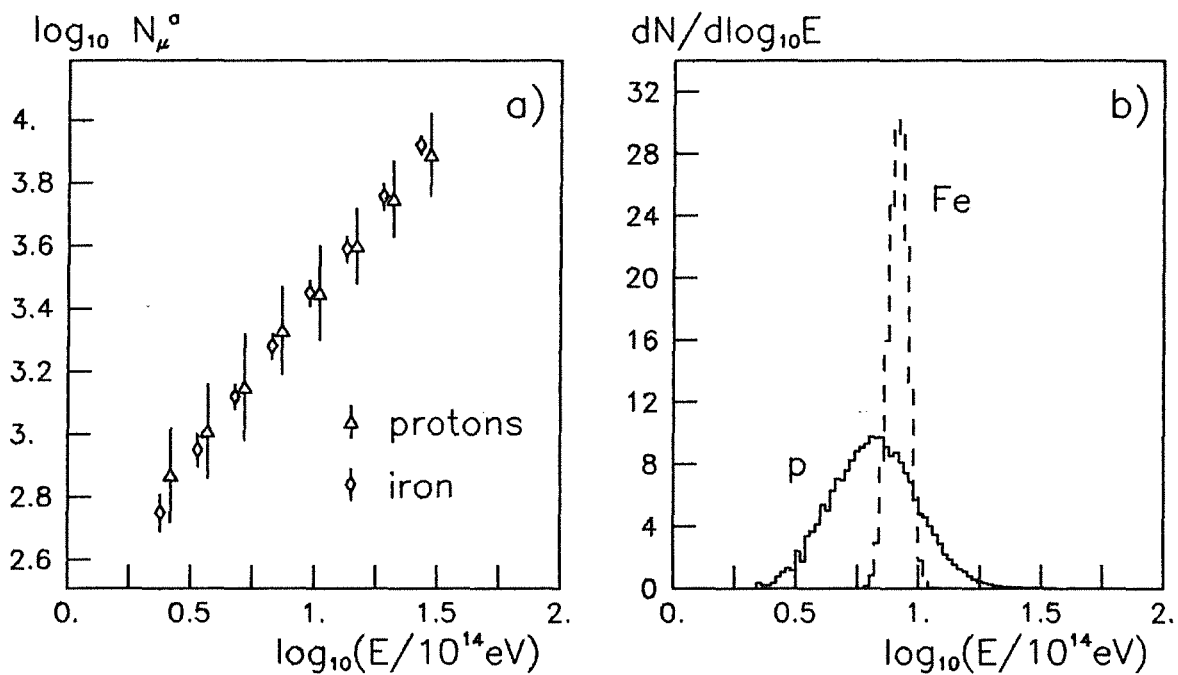


Fig. 3.5a Number of muons inside the array versus energy for p and Fe.

3.5b Energy spectrum contributing to a narrow range in N_μ^a for p and Fe showers.

Fig. 3.5a shows the correlation between the primary energy, E_0 , and the number of muons falling into the KASCADE array, N_μ^a . The latter turns out to be proportional to the primary energy. In fig. 3.5b the energy spectrum is shown contributing to a narrow range of N_μ^a .

Using N_μ^a as a measure for the primary energy gives an accuracy of $\approx 50 \%$ for protons and 10% for iron showers.

3.3.2.3 Electrons and photons

The electromagnetic component of an EAS originates primarily from π^0 decays. Neutral pions being produced in the lower part of the atmosphere can give measurable electrons and photons at the observation level. So the same arguments as for hadrons apply. For proton showers there are more electrons to be detected because there are more hadrons reaching the ground.

3.3.3 How to separate different primaries ?

A first attempt to identify air showers from different primaries was performed on the basis of 3 observables: the number of muons N_μ^a , the number of electrons N_e^a (both inside the KASCADE array) and the energy sum ΣE_h of all hadrons above 10 GeV having a distance ≤ 5 m from the shower axis. For convenience the decimal logarithms of these variables have been used. In tab. 3.1 the mean values and root mean squares of these observables are given for different primaries and different energies.

Tab. 3.1 Dependence of different observables on primary energy and particle type.

E_0 [eV]	Prim.	$\log_{10}N_e$	$\log_{10}N_\mu^a$	$\log_{10}\Sigma E_h^{5m}$
$2.5 \cdot 10^{14}$	p	4.47 ± 0.25	2.87 ± 0.15	3.56 ± 0.69
	^{16}O	4.07 ± 0.15	2.85 ± 0.08	2.88 ± 0.54
	^{56}Fe	3.73 ± 0.14	2.75 ± 0.06	2.18 ± 0.62
$5 \cdot 10^{14}$	p	4.82 ± 0.21	3.15 ± 0.17	4.04 ± 0.49
	^{16}O	4.49 ± 0.13	3.16 ± 0.06	3.50 ± 0.33
	^{56}Fe	4.24 ± 0.10	3.12 ± 0.04	2.93 ± 0.44
10^{15}	p	5.21 ± 0.22	3.45 ± 0.15	4.49 ± 0.45
	^{16}O	4.92 ± 0.11	3.48 ± 0.06	4.07 ± 0.28
	^{56}Fe	4.70 ± 0.07	3.45 ± 0.04	3.66 ± 0.27
$2 \cdot 10^{15}$	p	5.59 ± 0.19	3.75 ± 0.12	4.87 ± 0.34
	^{16}O	5.29 ± 0.11	3.78 ± 0.05	4.51 ± 0.20
	^{56}Fe	5.12 ± 0.07	3.76 ± 0.04	4.24 ± 0.15

One can see nicely that, at fixed energy, the number of muons falling into the array is the same for all primaries, whereas when increasing the energy by a factor of 2 the number of muons rises by a factor of 2 as well (i.e. $\log_{10}(N_\mu^a)$ rises by 0.3).

There is as well a rise of $\log_{10}(N_e)$ with energy but because of different numbers for different primaries a Fe shower exhibits the same number of electrons as a

proton shower at around half the primary energy. The differences between p- and Fe showers at the same energy in N_e are about a factor of 3.

The differences in the energy sum are even bigger but the fluctuations are big as well. With increasing energy the hadron measurement becomes more and more precise.

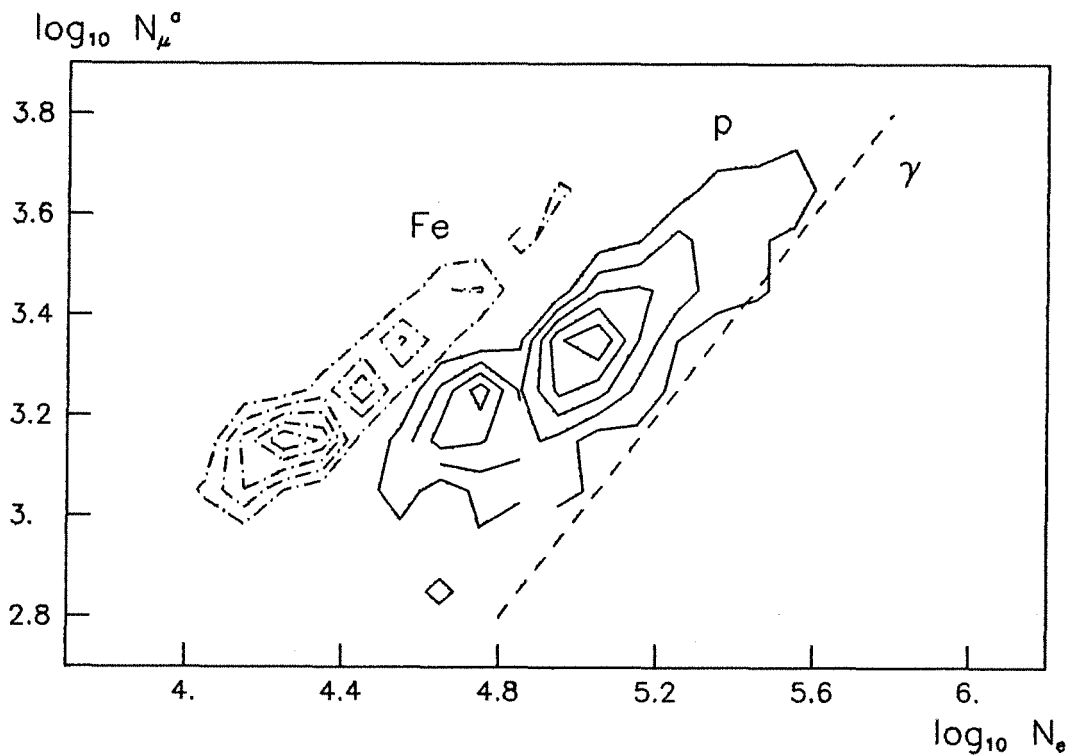


Fig. 3.6 Showers originating from p and Fe with respect to N_e^a and N_μ^a .

As mentioned above the primary energy of the showers was varied from $2.5 \cdot 10^{14}$ to $2.8 \cdot 10^{15}$ eV. The number of electrons and muons of these showers were determined and plotted in fig. 3.6. The steeply falling energy spectrum ($E^{-2.7}$) was taken into account. One sees the regions where Fe and p showers are enriched and recognizes the big fluctuations of the p-induced showers. There is even a tail of proton showers reaching the dashed line given by $N_\mu/N_e = 0.01$, indicating where photon induced showers would be expected.

The distributions of $\log_{10}(N_e)$ for a narrow band in $\log_{10}N_\mu$ ($3.5 \leq \log_{10}N_\mu \leq 3.7$) are given in fig. 3.7 showing the peaks of Fe and p showers separated with a small overlap. Fig. 3.7a displays the situation when the complete area would be covered with detectors, i.e. a detection efficiency of 100 % was assumed. In fig. 3.7b we included the limited sampling of electrons and muons of 2 % and 3 %, respectively, causing the band of detected muons to come down to $2 \leq \log_{10}N_\mu^{\text{det}} \leq 2.2$. Still the peaks are clearly separated and the width of the distributions stays almost

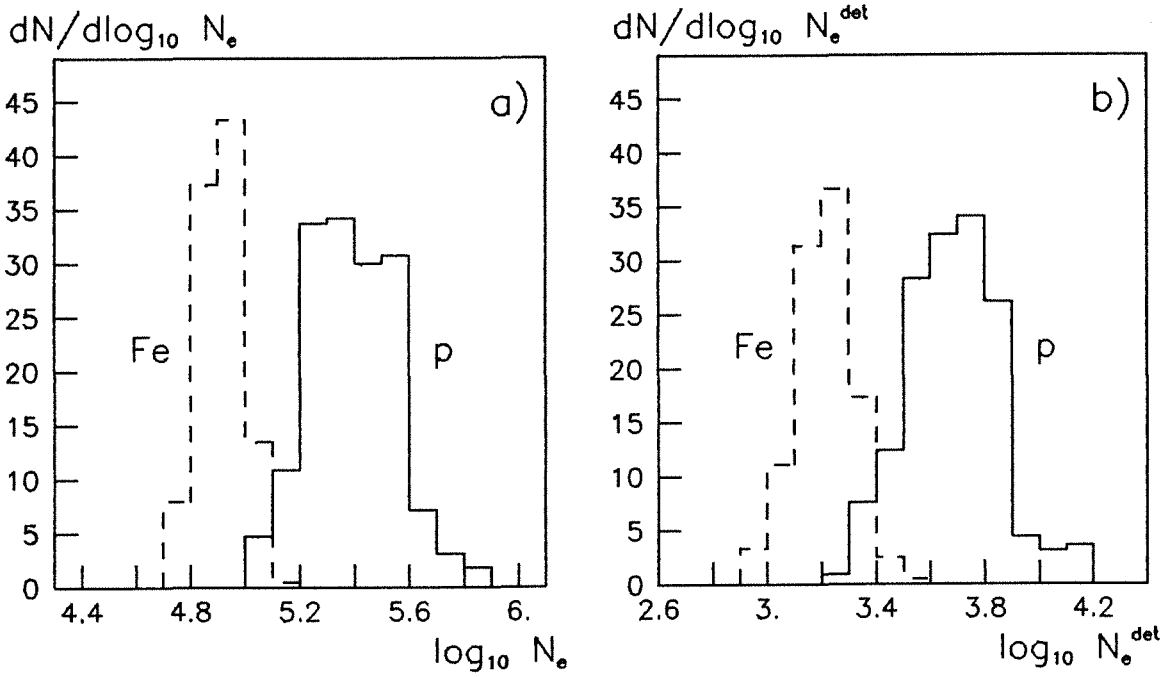


Fig. 3.7 Distributions of N_e for a fixed range of N_μ
 a) not including limited coverage; $3.5 \leq \log_{10} N_\mu^a \leq 3.7$
 b) including 2 % and 3 % coverage, for electrons and muons,
 respectively; $2.0 \leq \log_{10} N_\mu^{\text{det}} \leq 2.2$.

constant. This shows the intrinsic fluctuations dominating over the statistical ones for the sampling of our experiment.

For the range of observed muons between $2.0 \leq \log_{10} N_\mu \leq 2.2$, i.e. for a limited region in primary energy, the showers are classified according to their electron number N_e and the energy sum ΣE_h of the hadrons. The corresponding plot is shown in fig. 3.8. Clearly the regions of p and Fe can be separated and even the oxygen showers can be located.

Assuming a relative composition of p: ^{16}O : ^{56}Fe of 6:1:1.75, as extrapolated from lower energy measurements [5, 6], and projecting the plot along the straight line, indicated in fig. 3.8a, one obtains the histogram in fig. 3.8b. The iron peak is nicely separated from the protons. Placing the cut to enrich Fe-showers in a way that 90 % of the irons are identified correctly, only 14 % of the oxygen and proton showers are misidentified as iron. The signal to background ratio is 6.3.

Without using the hadron information the iron efficiency would be 85 % and the background amount to 17 %, leading to a signal to background ratio of 4.9.

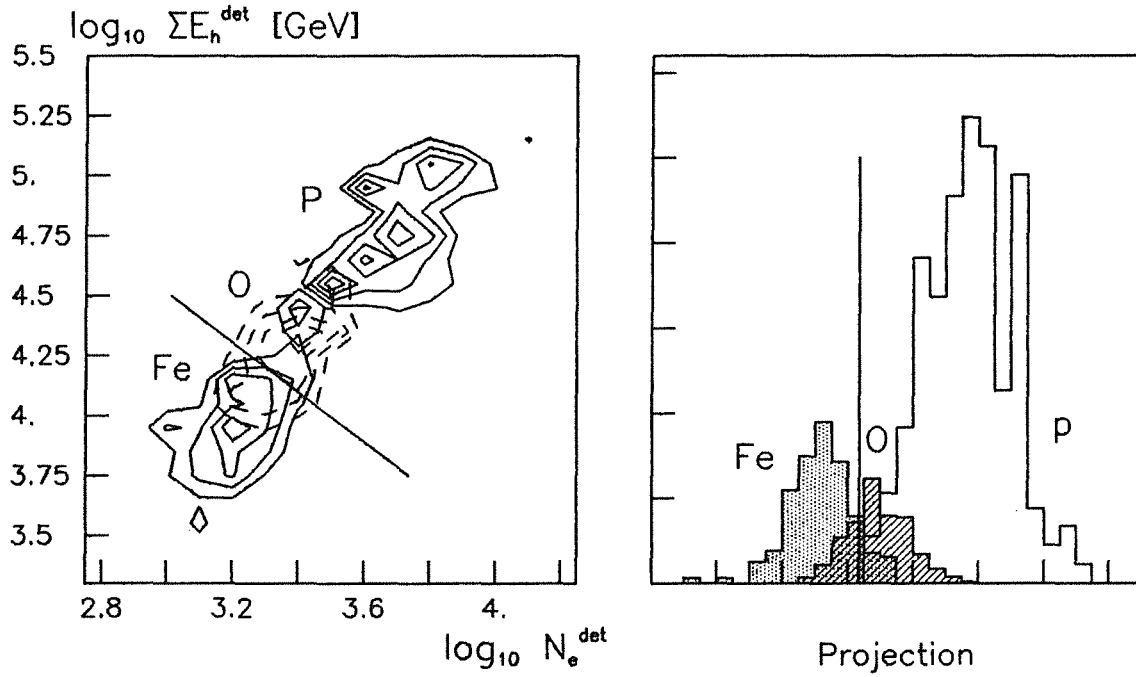


Fig. 3.8 N_e^{det} versus ΣE_h for showers with $2.0 \leq \log_{10} N_\mu^{\text{det}} \leq 2.2$ of different primaries.

With increasing energy the fluctuations of the energy sum of the hadrons becomes quickly smaller and the separation improves. For a number of detected muons between $2.2 \leq \log_{10} N_\mu^{\text{a det}} \leq 2.4$ the signal to background ratio is 7.7.

Showers incident at a zenith angle of 20° have been investigated as well. Tab. 3.2 shows how the observables compare for inclined and vertical showers. The absolute values decrease, the fluctuations increase slightly, but the differences between p and Fe persist.

Tab. 3.2 Dependence of different observables at fixed energy ($1 \cdot 10^{15}$ eV) on the shower zenith angle and on the particle type.

	Protons		Iron	
	$\Theta = 0^\circ$	$\Theta = 20^\circ$	$\Theta = 0^\circ$	$\Theta = 20^\circ$
$\log_{10} N_e$	5.21 ± 0.22	5.11 ± 0.25	4.70 ± 0.07	4.52 ± 0.10
$\log_{10} N_\mu^{\text{a}}$	3.45 ± 0.15	3.43 ± 0.15	3.45 ± 0.04	3.40 ± 0.05
$\log_{10} \Sigma E_h^{5\text{m}}$	4.49 ± 0.45	4.37 ± 0.45	3.66 ± 0.27	3.35 ± 0.39

4. The detector array

An extended field of distributed detector stations is used to determine the following properties of extensive air showers :

- the number of particles in the soft component of the showers (electrons, positrons, photons) and their lateral distribution
- the number of muons outside the shower core and their lateral distribution
- the direction of the primary particle by measurement of the inclination of the shower disc using the method of relative arrival times
- the position of the shower core

In addition, the array will deliver a trigger signal for the detector electronics of the **KASCADE** central calorimeter.

For this task 1264 scintillation detectors for the electron / photon component and 316 muon detectors (below a heavy shielding) will be used. These detectors are arranged on a rectangular grid ($d \sim 13$ m) covering an area of 200 x 250 m.

4.1 Layout of the array

Extensive Monte Carlo calculations have been carried out to optimize the **KASCADE** array. The size of the array, the sampling, the detector spacing and the necessary detector performance are mainly determined by the properties of the electromagnetic part of the showers. The program package **GEANT 3** [53] has been used to simulate electromagnetic cascades induced by high energy photons in the atmosphere and to investigate the properties of such showers at ground level and the response of the proposed detector system to these showers.

One important result of these calculations is that most shower parameters (particle numbers, age, etc.) are subject to large fluctuations. This is in agreement with the **CORSIKA** simulations for hadron induced showers and with the results of many other investigations. Therefore, it is mandatory to simulate a statistically significant number of single events to predict average shower properties reliably. It is even more important to realize that the accuracy of the reconstruction of a single event will normally be dominated by the shower fluctuations. This determines the degree of quality which has to be achieved by the detectors.

Fig. 4.1 shows the calculated radial density distribution of electrons and photons in a photon induced air shower at 110 m above sea level for an incident energy of $5 \cdot 10^{14}$ eV. All calculations have been carried out with an energy cut of 3 MeV.

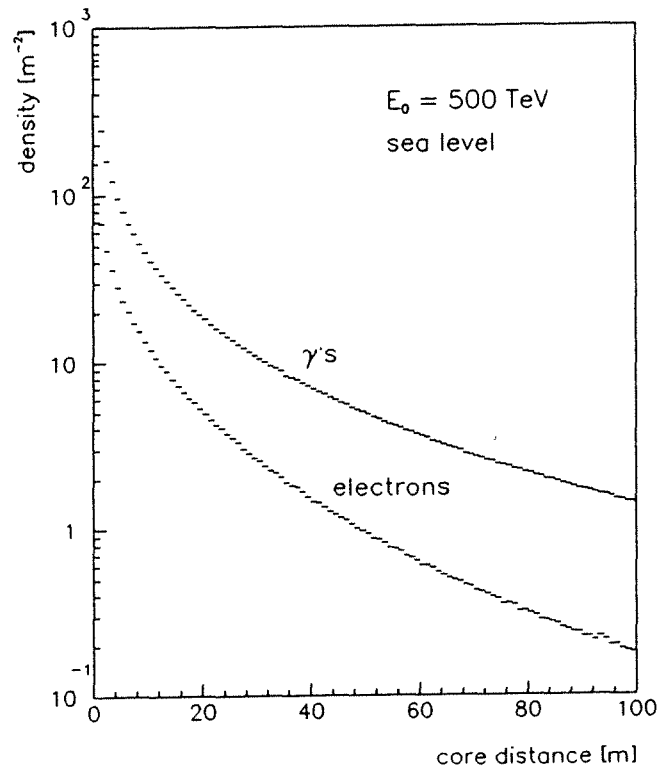


Fig. 4.1 Radial density distribution of electrons and photons with $E \geq 3 \text{ MeV}$ for photon induced showers at an energy of $5 \cdot 10^{14} \text{ eV}$.

The effective size of the electromagnetic component of an air shower can be defined by the core distance, at which the probability of a detector hit equals 0.5. At the energy threshold of the **KASCADE** experiment ($3 \cdot 10^{14} \text{ eV}$) this corresponds to a radius of about 40 m. To achieve a good reconstruction of events this area has to be covered by a sufficiently large number of detectors. In similar air shower experiments the density of the lateral sampling is far below 1 % [54, 25]. For the **KASCADE** array a 2 % sampling is planned to compensate for the lower particle density near sea level compared to mountain altitude. Extensive air showers at sea level exhibit an electron / photon ratio of about 1 to 6. Therefore, it is important to obtain a high detector efficiency for photons by using a lead converter foil.

The energy spectra of the shower particles (fig. 4.2) show a broad distribution up to energies of several GeV. The shape of the spectra is nearly independent on the incident energy. The photon excess is mainly in the energy range below 100 MeV. These energy spectra are 'harder' near the shower core and 'softer' at larger core distances. This radius dependence of particle energies, as shown in fig. 4.3, is important for the reconstruction of shower events and for the feasibility of muon detection by employing a thick absorber plate for the electrons and photons.

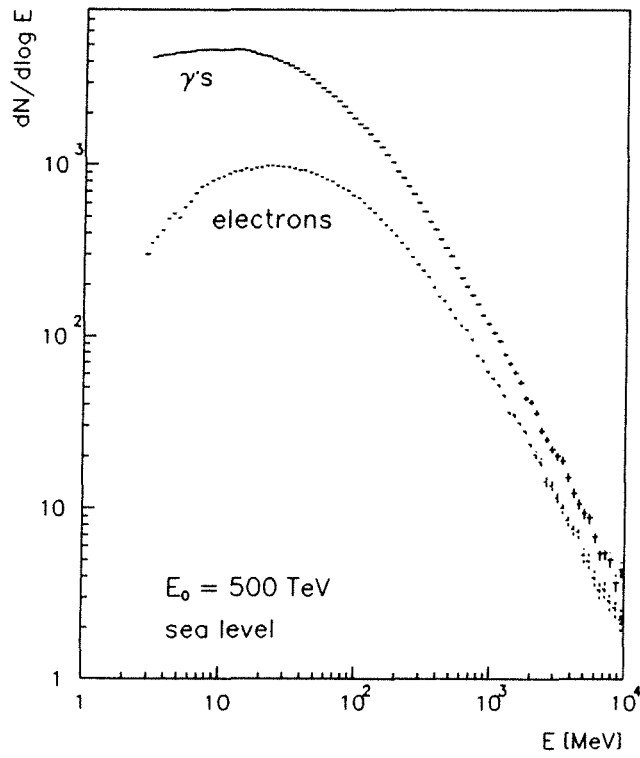


Fig. 4.2 Energy spectra of electrons and photons in a photon induced air shower at $5 \cdot 10^{14}$ eV.

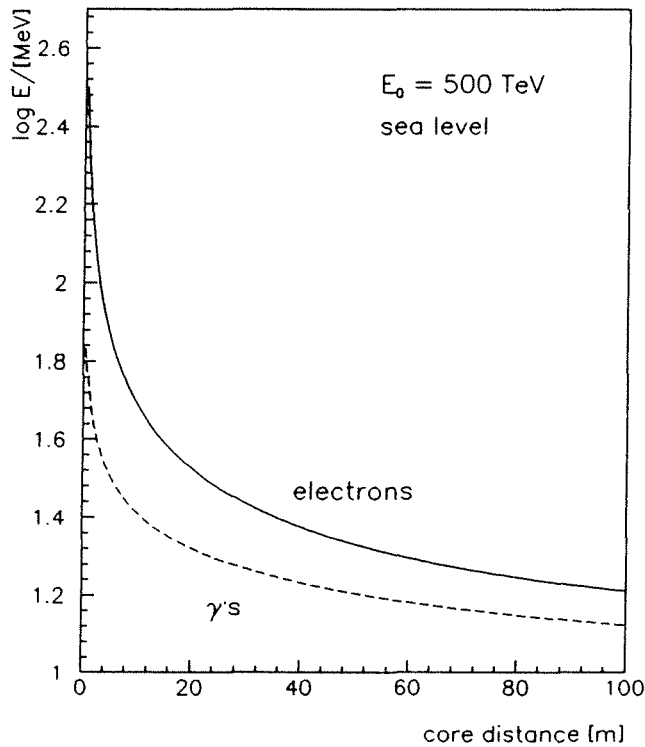


Fig. 4.3 Mean values of particle energies in photon induced air showers as a function of core distance.

The measurement of relative arrival times with an array of detectors is used in many air shower experiments to determine the direction of the primary particle.

With this method angular resolutions of about 1° have been achieved. With high lateral sampling and good time resolution it seems possible to obtain an angular resolution of $\leq 0.2^\circ$ at primary energies $\geq 5 \cdot 10^{15}$ eV.

The simulations of the particle arrival times show that the air showers are quite extended in space and time. However, the main information lies in the area near to the core and in the first 5 ns. A closer look on the time spectra reveals a different behaviour of electrons and photons. The front of the shower is formed dominantly by the photons. The distribution in time is wider for the electrons. For the reconstruction of the shower front a good photon efficiency is hence very important.

For the KASCADE array fast scintillation detectors will be used for the shower particles and the method of relative arrival times will be employed for the determination of the shower direction.

4.2 Detectors for the electron / photon component

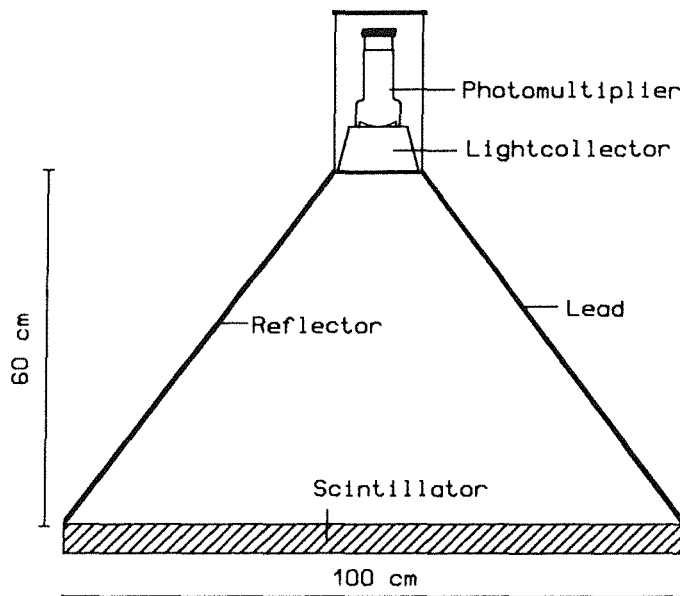


Fig. 4.4 Schematic drawing of the detector design for the electron / photon component of extensive air showers.

The design of the detectors for the electron / photon component of the shower has to be a compromise with respect to: large area, good time resolution, reasonable energy resolution, high dynamic range and low cost per unit area. Monte Carlo simulations and extensive prototype work have led to the detector design shown schematically in fig. 4.4. The scintillator will have the shape of a cylindrical slab of 100 cm \varnothing . The corners of a quadratic sheet would make the time resolution

considerably worse. A thickness of 4 cm is sufficient if a high quality scintillator is used.

In a series of investigations more than 25 different scintillator materials from 8 manufacturers have been tested. Using penetrating cosmic muons and gamma ray sources we determined light output, decay time, temperature dependence, and light attenuation length. Following these tests several high quality plastic scintillators (like NE 102A) are well suited technically, but the prices are considerable. Liquid scintillators are much cheaper and quite easily tailored to the needs of a specific experiment. A third option is the production of a custom-made cheap scintillator out of clear polystyrene, a primary fluor and a wavelength shifter. This method is presently investigated in collaboration with MPI, Munich. For the prototype part of the experiment we will make use of a fast, inexpensive liquid scintillator with high light output.

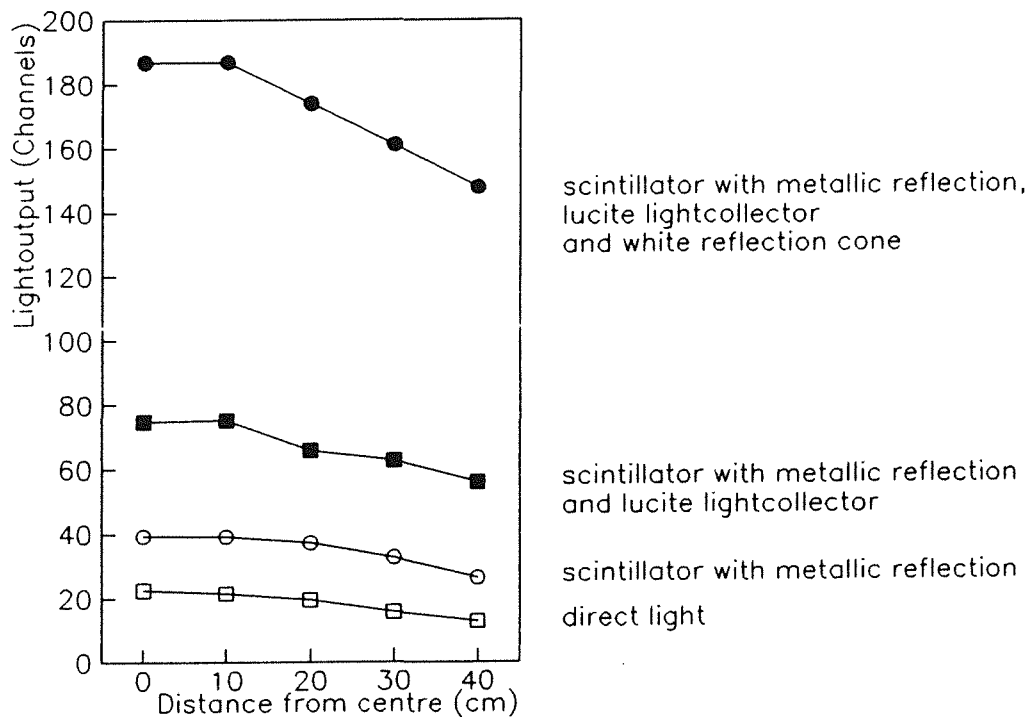


Fig. 4.5 Light collection efficiency for penetrating muons as function of the radial position of the interaction. Metallic reflector, white cone, and the lucite light collector increase the number of photoelectrons considerably.

In extensive prototype measurements we have tested many different geometries, photomultiplier tubes and light collection schemes. In parallel, Monte Carlo calculations have been carried out covering the production, transport and collection of the scintillation light. We were able to optimize both the timing

properties by increasing the direct light as well as the total photon number by various reflection schemes.

At the bottom of the scintillator a highly reflecting material increases the direct light by a factor of nearly two. For better light collection a lucite cone is connected to the phototube. This cone gives an 80 % enhancement to the efficiency of a 3" PM tube for 10 % of the cost.

The container is made out of stainless steel with a glass window on the top side, sealed by a viton O-ring. The photomultiplier is a 3" diameter - 10 stage tube with signals taken from the anode and from the 8th dynode to get a sufficiently large dynamic range. On the inner side of the conical detector housing a white diffuse reflector is used for better uniformity of the integrated light. The improvement of the light collection by these various steps is demonstrated in fig. 4.5 for the light produced by muons penetrating the detector at different radial positions.

For a minimum ionizing particle we get about 25 photoelectrons using 4 cm of a high grade scintillator and a 3" photomultiplier tube. The detector as described above has an area of 0.78 m^2 , an energy resolution of 25 % for minimum ionizing particles, and a time resolution better than 0.8 nsec.

4.3 Detector stations

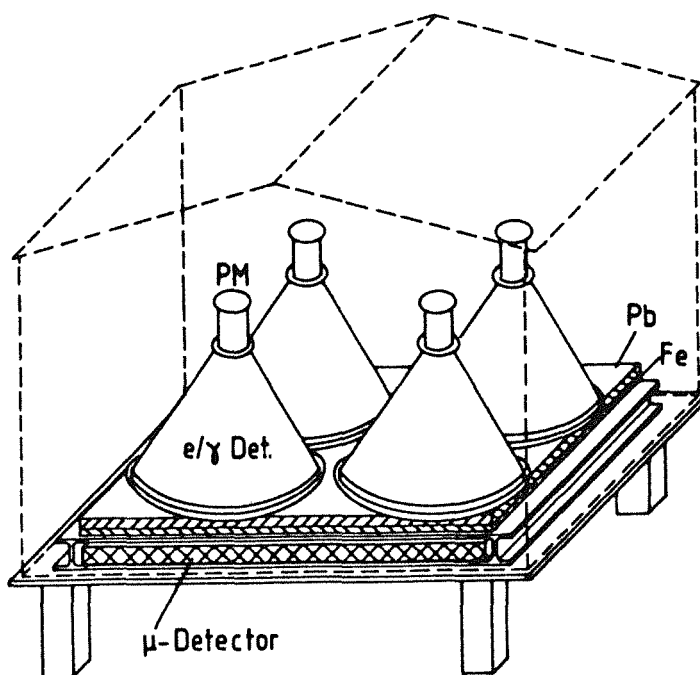


Fig. 4.6 Schematic view of a detector station containing four detectors for the electromagnetic component on top of 20 r.l. of lead / iron shielding and a 3.2 m^2 muon detector below.

Four detectors are combined in a detector station. Commercially available metallic garden sheds with an area of 2.3 m x 2.7 m are used for weather protection. Each shed is supported by a concrete platform 0.5 m above ground level. Air flow is enabled for convective cooling at high outside temperatures. No further installations are foreseen in the detector stations. Fig. 4.6 shows an artists view of a detector station with the 4 electron / photon detectors on top of a 200 x 200 cm lead / iron plate. The thickness of the plate is 4 cm of iron and, on top, 10 cm of lead, corresponding to a total of 20 radiation lengths. This plate is used as an absorber for the electrons and photons in the air shower. The muon detectors (described in the following sect.) are placed directly below the heavy shielding.

The total weight of a detector station is about 8 tons.

4.4 Muon detection

An important task for the **KASCADE** array is the measurement of the muon component in extensive air showers. In hadronic showers muon numbers are 2 % to 20 % of the electrons depending on energy and mass of the primary particle and, especially at energies below 10^{16} eV, on the zenith angle of the event. For photon induced showers the muon content should be only about 0.2 % of the electron number if the photonuclear cross section does not exhibit a surprisingly strong rise at ultrahigh energies. The muon component is characterized by a wider lateral distribution. The radius parameter corresponding to the Molière radius of 80 m for the electrons is of the order of 300 m for muons. If the shower core hits the array, only 20 % to 40 % of the muons fall inside. Therefore, a large sampling for muon detection is necessary. We plan to install 316 detectors of 3.2 m² each in the array, shielded by 20 r.l. lead / iron. This thickness corresponds to a muon threshold of about 300 MeV. Additional muon chambers (300 m²) will be placed below the central calorimeter with a muon threshold of about 2 GeV.

For the muon detectors in the array two different detector designs have been considered. The first one consists of four scintillator sheets read out by four 1.5" PM tubes using wavelength shifter (WLS) bars on all edges of the scintillators. This design is shown schematically in fig. 4.7. To achieve good spatial uniformity, a scintillator material with large light attenuation length has to be used. Fast decay time is less important, because the green fluors of the WLS are relatively slow, anyhow. We have tested a number of materials for this application. NE 114 or a similar scintillator would be a good solution. WLS material is available from different suppliers (BBQ, Y7, NE 172, etc.) with only slight differences in quality.

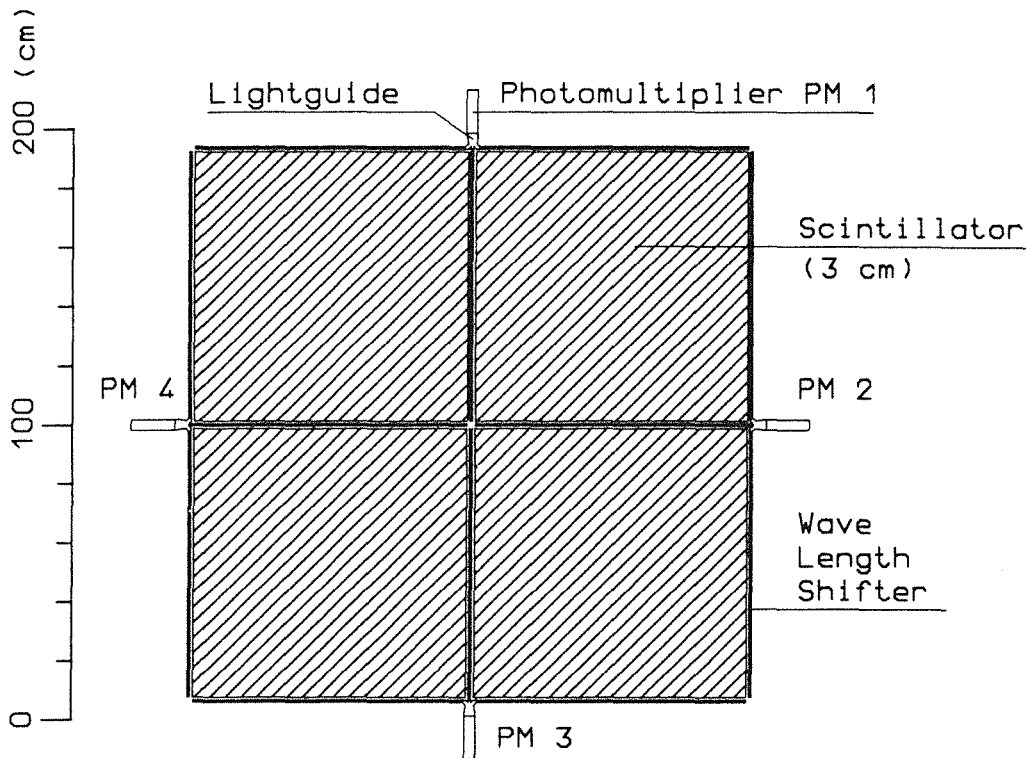


Fig. 4.7 Scintillator muon detector, 3 cm thickness, with wavelength shifter readout.

For the PMs the cathode should have enough sensitivity in the green wavelength range (500 - 550 nm) to obtain good resolution. Our prototype measurements show that this seems to be no technical problem. The result of a test measurement using penetrating muons is shown in fig. 4.8 for a 90 x 90 x 2 cm³ sheet of scintillator BC 416 with Y7 wavelength shifters on all edges. Good spatial uniformity of the pulse heights is very important to enable a high threshold (~ 3 MeV) for the muon detectors without loss of muon efficiency.

The problem of 'faked' muons by energetic electrons and photons in the shower punching through the absorber plate can be reduced considerably by a high threshold. Extensive Monte Carlo calculations using the **GEANT 3** code have been carried out for the set-up described above to investigate this problem quantitatively. The result is shown in fig. 4.9 as a function of core distance. It is evident that near the shower core the punch-through is a serious problem due to the high energies of many particles in this region (see fig. 4.3). In addition, the hadrons in the core would generate fake signals in the muon detectors. Using an off-line radius cut of ~ 20 m together with an energy threshold of 3 MeV reduces the fake signals to a tolerable level. The total muon efficiency of the array is reduced only slightly (15 %) by this radius cut.

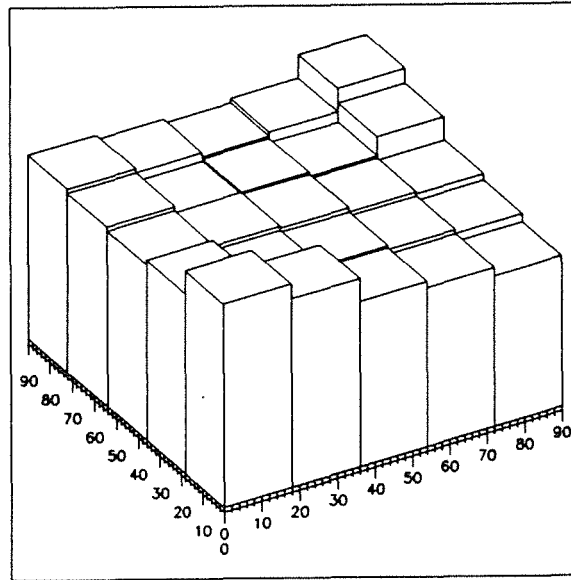


Fig. 4.8 Spatial dependence of pulse heights for muons in a 2 cm thick scintillator sheet of BC 416, read out by Y7 wavelength shifters.

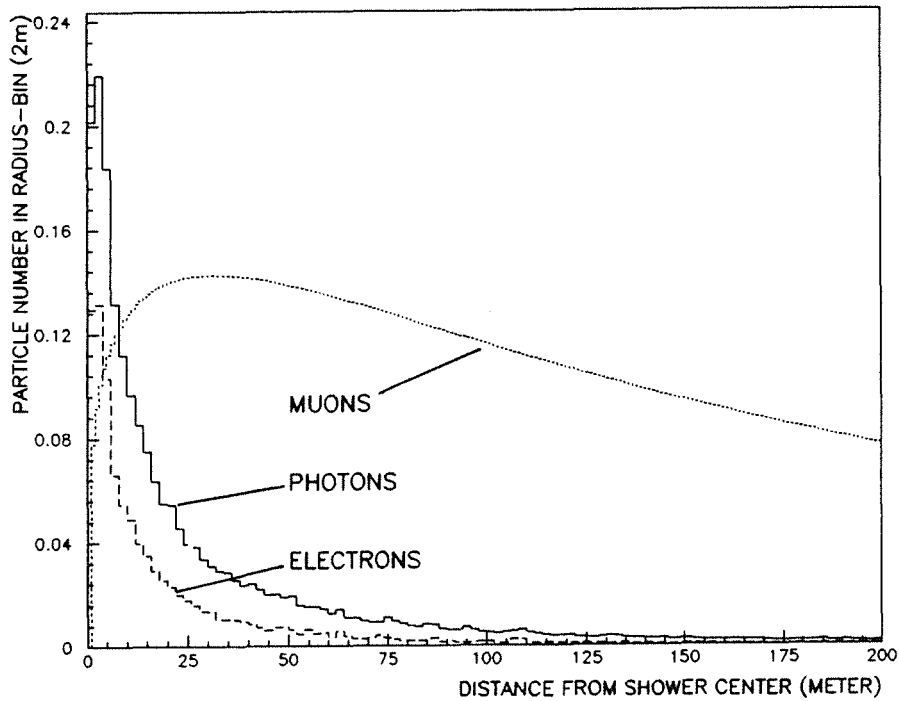


Fig. 4.9 Radial dependence of detected muons and of the punchthrough of energetic electrons and photons through a 20 r.l. absorber plate in a 10^{14} eV proton induced shower.

For hadronic showers the punchthrough increases the registered number of muon signals by 5 to 15 %, depending on the energy and the mass of the primary particles. In the shower reconstruction this 'error' can be calculated and corrected with good reliability. We conclude that the problems connected with punchthrough are small compared to the effects of the intrinsic shower

fluctuations. The main drawback of the scintillator design is the relatively high price per unit area.

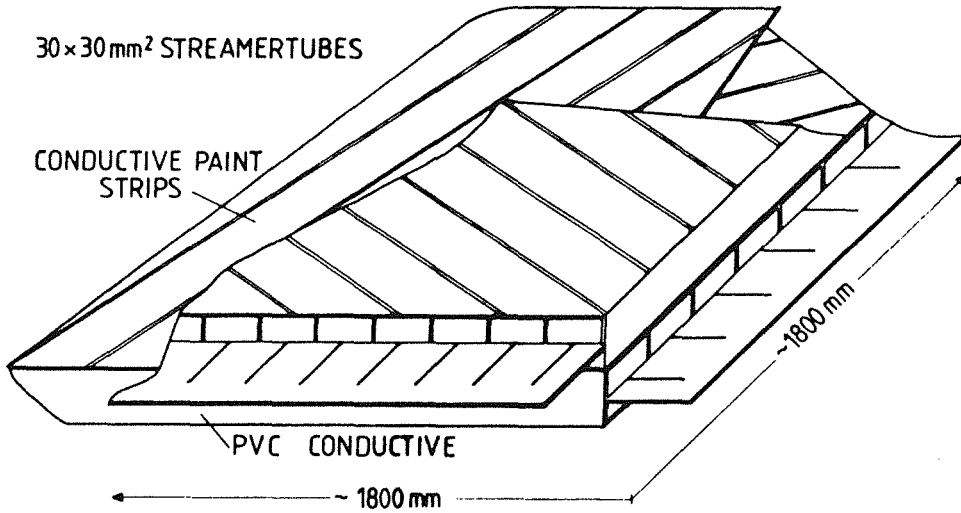


Fig. 4.10 Two layer streamer tube muon detector design with strip readout. The tube size is 3 x 3 x 180 cm.

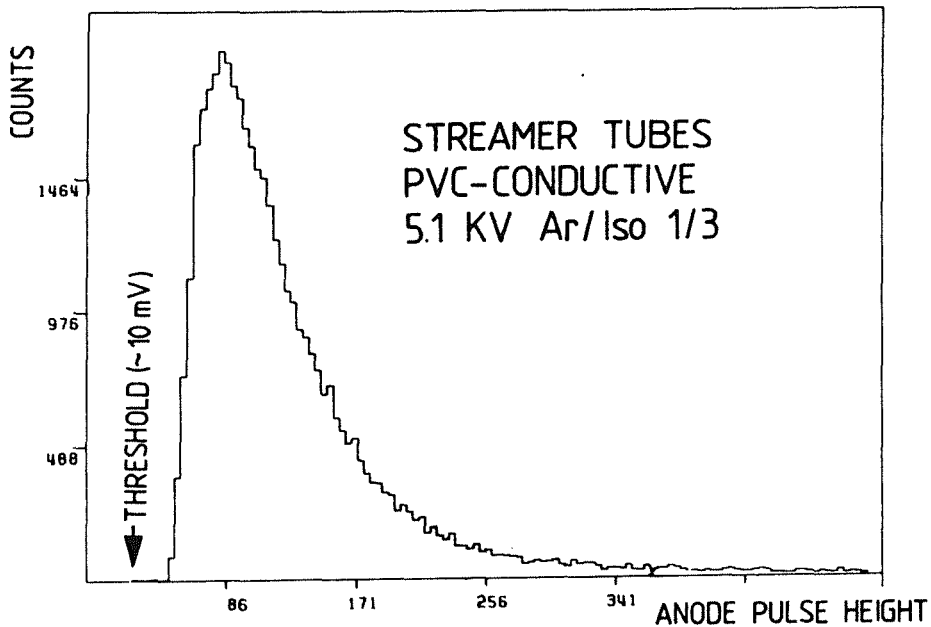


Fig. 4.11 Signal pulse height distribution of limited streamer tubes in the plateau region.

Therefore, a different approach has been investigated. It contains two layers of limited streamer tubes [55] at the position below the lead / iron plate. Streamer tubes are used in many recent experiments where large detection areas are needed

at a reasonable price, especially in high energy physics. Much expertise and technical information is available on the production and the operational features of streamer tubes. These tubes are well suited for muon detection. Photon sensitivity is around 1 % for ^{60}Co photons and less for keV photons depending on the tube wall thickness. Two layers of streamer tubes in coincidence are rather insensitive to punchthrough photons.

We have studied different tube designs, readout methods and gas mixtures. In this process, commercially available and custom made tubes have been investigated. Especially the use of conductive plastic as base material seems promising. For the readout, cathode strips can be produced in an economic way by means of conductive paint. The result is, briefly, that streamer tubes can be built and read out for a lower price compared to the scintillator and be used with good reliability at least in the laboratory. The field operation in detector stations of a large number of streamer tubes, especially at low temperatures, makes it necessary to improve the commonly used gas handling systems and to develop a reliable gain stabilization for these tubes. In addition, the production, the testing and the operation of streamer tube muon detectors would require a much larger effort with respect to man power compared to the scintillator solution.

4.5 Structure of the array

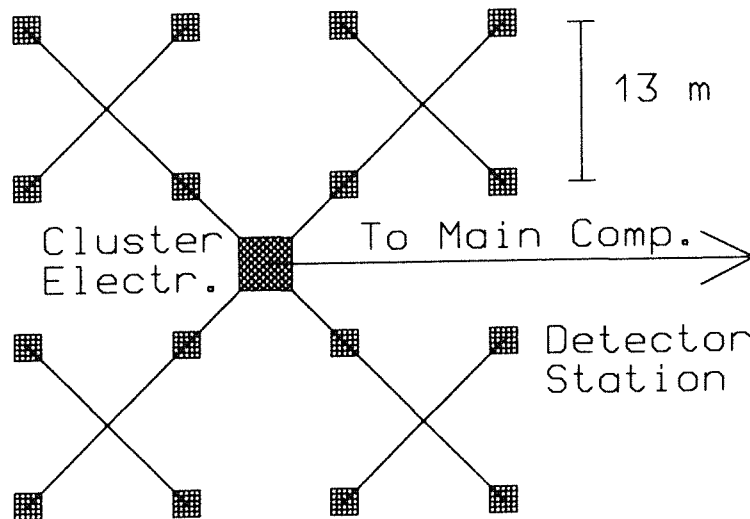


Fig. 4.12 Electronic link between the sixteen detector stations which form a cluster. All supplies electronics etc. are located in the 17th station.

The stations form a rectangular grid of 13 m spacing. Sixteen detector stations are combined in a cluster as shown schematically in fig. 4.12. All stations are linked to

a central station which contains all supplies, the front-end electronics including the fast trigger logic and the local intelligence. The cluster is taking data like a mini-array, the real time data acquisition is independent in each cluster.

The array consists of 20 clusters. Near the center of the array 4 clusters contain only 15 detector stations to leave enough space for the central calorimeter.

The central station of each cluster is connected to the main data acquisition and computer system via fiber optics data links and a fast trigger line. Data from different clusters are correlated using a synchronous 200 nsec time label, derived from a central absolute UTC clock. The arrival times of the shower particles are measured relative to this 5 Mc period for all electron / photon detectors in a cluster. The 200 ns time label is added to the data for each valid detector event in the cluster and transferred to the main data acquisition system when a data request is sent to the cluster. By this method uncorrelated background is reduced significantly. Uncorrelated signals from single muons allow on-line control of the stability of detector gain. A light pulser and fiber optics system is used to determine the relative signal delays in the electron / photon detectors, the cables and the front-end electronics.

The data acquisition system is described in more detail in chapt. 6.

4.6 Simulated array performance

For the analysis of the raw data and for event reconstruction a sound understanding of the detector properties is mandatory. A detailed simulation of the array and its components is important for the process of optimizing the detectors and structures during the phase of planning the experiment as well as for the development of methods of event reconstruction and for the interpretation of the data taken in the experiment.

For the **KASCADE** array simulations were carried out with the program package **GEANT 3**, which is widely used in high energy physics applications. It allows a detailed description of the different parts of a detector station with respect to their geometrical and material properties. The simulation of the detector response to an incident particle with well defined arrival time, direction, and energy is performed by explicitly tracking the particles through the detector components taking into account all relevant interactions with the detector material. The energy deposit in the scintillator is folded with the specific light output, the light collection efficiency, and the characteristics of photomultiplier tubes and electronics to get a simulated detector signal. Detector timing and pulse height information are derived from this signal.

If this method is combined with the detailed information from a simulated shower as input, the array response to an extensive air shower event can be simulated almost perfectly resulting in a list of raw data. These simulated data are analyzed in the same way as real data will be later. In this way the programs for data analysis can be tested and optimized.

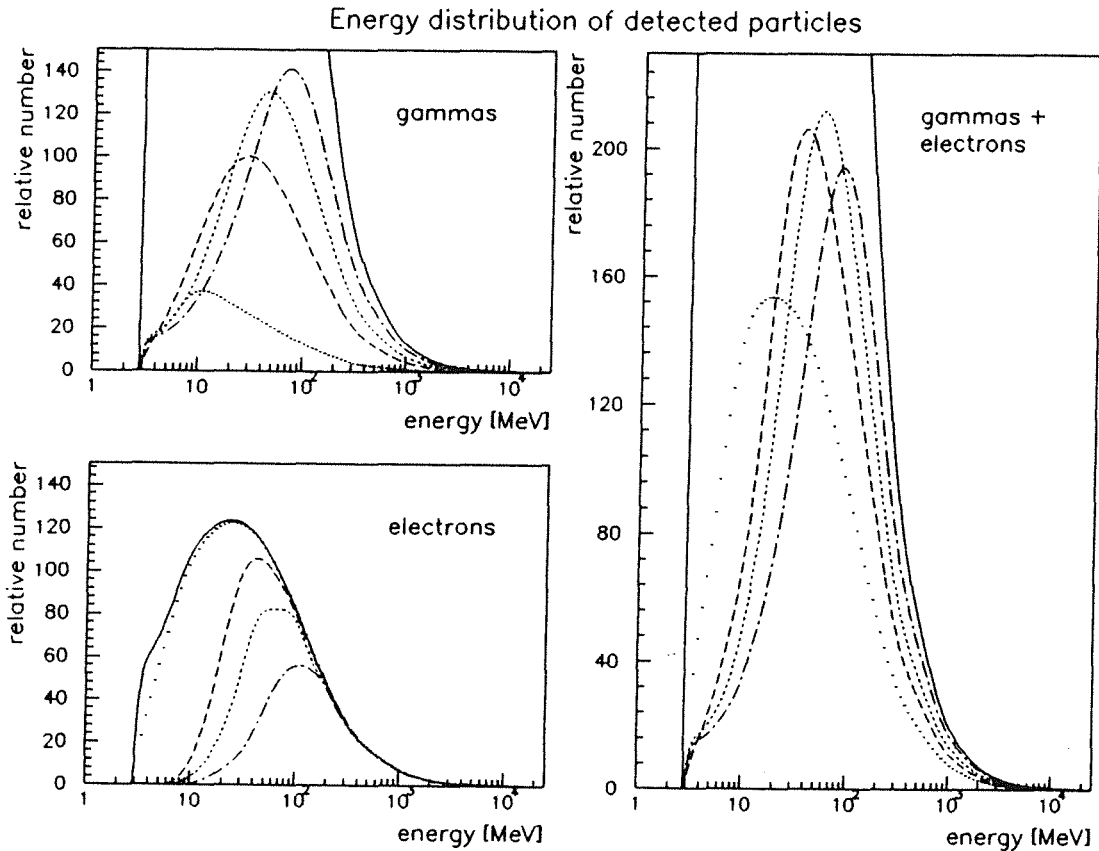


Fig. 4.13 Detector efficiency for electrons and photons as function of energy and lead converter thickness. The e/y energy spectra are folded in. The solid lines show the primary spectra, the different lead thickness is for : dotted line: no lead, dashed line: 2.5 mm, short dashed line: 5 mm and dashed-dotted line : 10 mm.

The first detail to be optimized was the lead converter foil thickness for the electron / photon detectors. Results of these calculations are shown in fig. 4.13. A lead sheet of about 5 mm (~ 1 r.l.) is sufficient to increase the photon efficiency considerably without implying too high a threshold for electrons. In the following discussions and calculations a lead thickness of 5 mm is used and an energy threshold of 3 MeV for both detector types is always assumed.

The array properties have been simulated up to now using photon induced showers incident vertically near the center of the array. When the total number of

electrons falling into the array is used as an effective size parameter, the dependence of the results on zenith angle and core position is only weak.

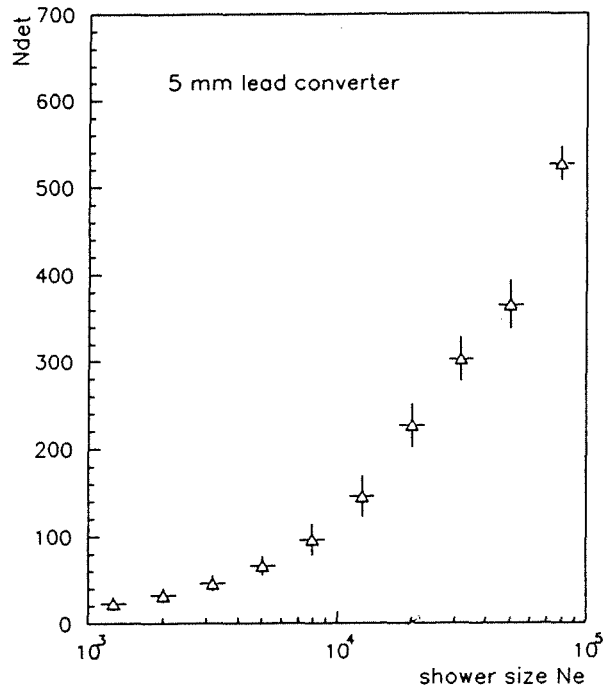


Fig. 4.14 Detector hits vs. total electron number in an air shower.

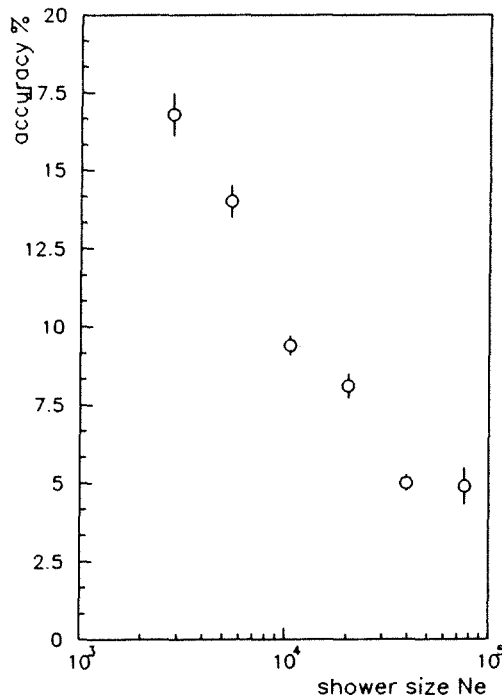


Fig. 4.15 Accuracy of shower size reconstruction as a function of electron number.

Fig. 4.15 shows the estimated accuracy of the reconstruction of the shower size N_e for particle numbers corresponding to the energy range up to 10¹⁵ eV. The main result is that the intrinsic shower fluctuations dominate and that the 2 % lateral sampling of the KASCADE array will be sufficient.

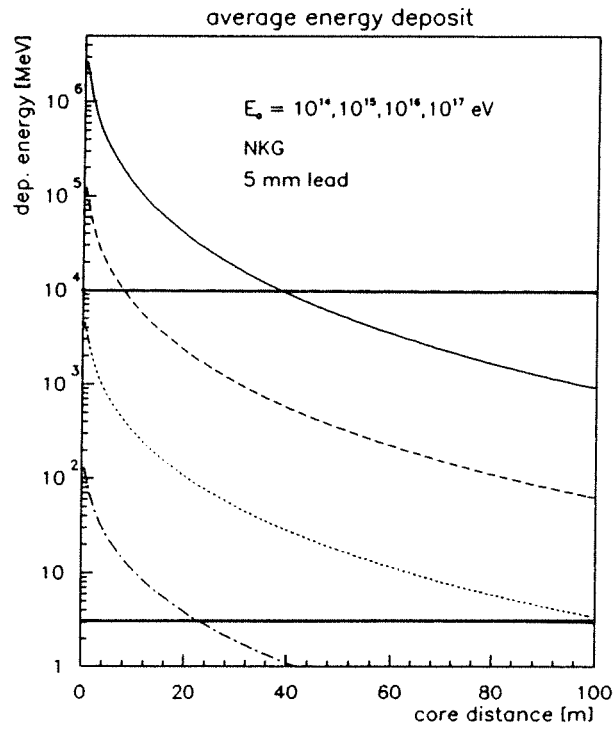


Fig. 4.16 Radial dependence of energy deposited in one scintillation detector for different primary energies. The horizontal lines indicate the lower energy threshold and the dynamic range of the detectors.

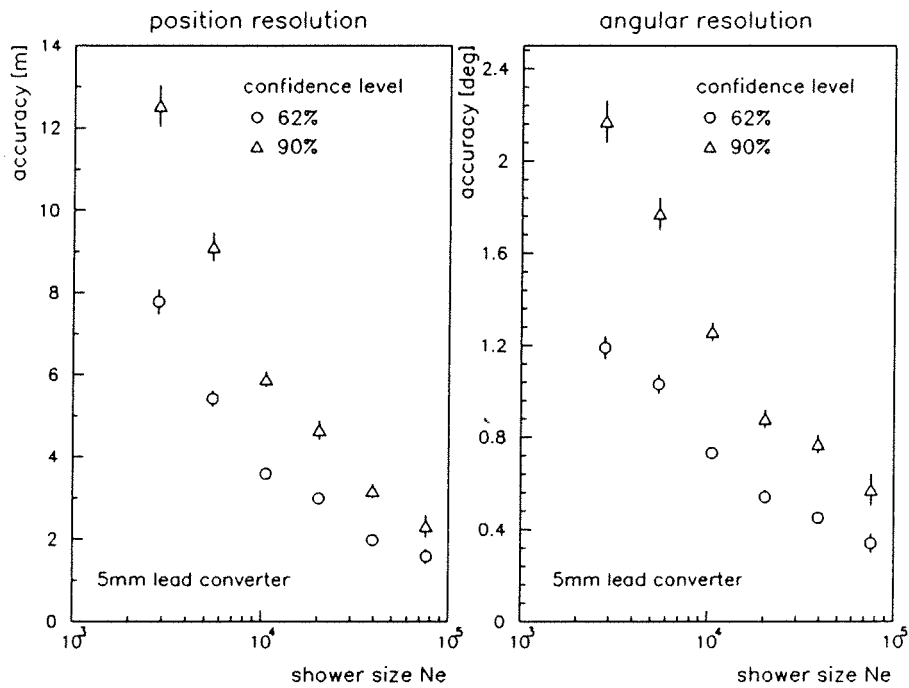


Fig. 4.17 Reconstruction accuracy of core position and shower direction as a function of electron number.

Another important result of the calculations is the dynamic range required for the electron / photon detectors to cover the primary energy range up to 10^{17} eV. The energy deposit in the scintillators is plotted in fig. 4.16. This result implies that a dynamic range of about 1 : 3000 is necessary for the detectors which can be achieved by using a signal from the 8th dynode of the PM in addition to the anode signal.

Of crucial importance, especially for the search for point sources of neutral UHE radiation, is the angular (and spatial) resolution of the array. The results of the simulations for these quantities are shown in fig. 4.17. The values refer to 62 % and 90 % confidence levels. This means, e.g., that for 10^5 particles in a shower (\geq 500 detectors fire) 62 % of the events fall inside a cone of 0.3° . The projected resolution would even be better by about a factor of 1.7 !

4.7 Event rates

For the full size of the KASCADE array (200 x 250 m) an accepted event rate of about 1 s^{-1} is anticipated. The total trigger rate from single clusters will be about 10 times higher. The energy range below 10^{15} eV dominates with more than 90 % of the events. Near the energy threshold of the array showers with larger zenith angles are suppressed. At higher energies the measurements can be extended to zenith angles of more than 30° and to showers with cores slightly outside the array. This increases the effective array area. Showers above 10^{16} eV are measured still with a rate of ca. 300 d^{-1} . For energies greater than 10^{18} eV we will get nearly 100 events a^{-1} . Rates at even higher energies could be improved by additional satellite clusters at larger distances from the array.

4.8 Search for UHE point sources

The search for cosmic point sources of ultra high energy radiation requires a large array area due to the expected flux and, in addition an excellent suppression of the isotropic background of hadronic showers. For the latter purpose a good angular resolution is crucial. The precise determination of the muon content in the air showers has long been proposed for identification of photon induced showers. Recent experimental evidence [16, 20, 57] is contradictory in this respect. Therefore, it seems even more important to measure the muon contents of these showers with better accuracy to investigate this interesting behaviour.

All experimental parameters (angular resolution, effective array area, zenith angle range, etc.) are strongly dependent on shower size i.e. on the energy of the incident particle. To calculate the sensitivity of a specific array for the search for

point sources one has to estimate the energy dependence of the neutral (photon ?) flux as compared to the normal hadronic cosmic ray flux. Most observations in the GeV to TeV range of source candidates indicate an E^{-2} differential spectrum. At PeV energies the experimental situation is more contradictory, but in overall agreement with an unsteady behaviour of the sources (bursts !). Therefore, the array sensitivity has to be calculated for both possibilities : a) photon emission in short bursts or b) a weak, but steady flux.

In these calculations one has to take into account the 'time of visibility' of an individual source candidate for the location of the experiment. In fig. 4.18 the band of visibility is shown on a galactic map for the **KASCADE** latitude (49°N) assuming a zenith angle $\leq 30^\circ$. The positions of several interesting objects are indicated. The daily observation time for the most prominent source candidates, Cygnus X-3 and Hercules X-1, is about 5 h. The Crab system can be seen only for 2.2 h each day. The larger zenith angle range at higher energies increases the observation time considerably.

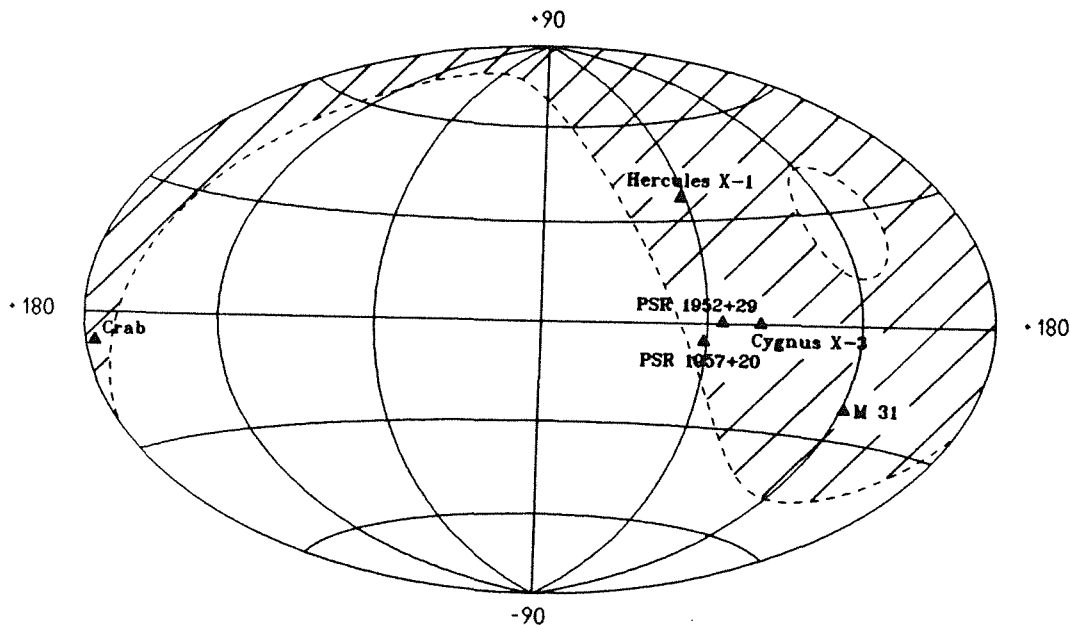


Fig. 4.18 Galactic map with several source candidates and the visibility band for zenith angles $\leq 30^\circ$ at 49°N .

Tab. 4.1 gives conservative estimates for the neutral flux which can be detected in 3 years of observation time with a statistical significance of 5σ or by at least 10 events on a negligible background. Φ is the source flux which can be separated from the hadronic background by the experimental angular resolution alone. Φ_μ is the corresponding flux, if the hadronic background can be reduced by selection of muon-poor showers. The flux Φ_B indicates the sensitivity of the **KASCADE** array

Tab. 4.1 Estimated detection limits of point source fluxes (see text)

	10^{15} eV	10^{16} eV	10^{17} eV
Φ [$\text{cm}^{-2}\text{sec}^{-1}$]	$1.2 \cdot 10^{-14}$	$6 \cdot 10^{-16}$	$2 \cdot 10^{-16}$
Φ_{μ} [$\text{cm}^{-2}\text{sec}^{-1}$]	$2.0 \cdot 10^{-15}$	$4 \cdot 10^{-16}$	$2 \cdot 10^{-16}$
Φ_B [cm^{-2}]	$1.3 \cdot 10^{-8}$	$8 \cdot 10^{-9}$	$6 \cdot 10^{-9}$

for short bursts of neutral radiation, i.e. the detection of ≥ 10 events within a few hours. These estimates do not contain any correlation with time variability of the sources like X-ray ephemerides. The absolute timing of the KASCADE experiment ($\sim 1\mu\text{s}$) will enable an off-line phase analysis with good accuracy.

Due to the high sampling of 2 %, the good angular resolution, and the large area for muon detection the KASCADE array will be able to contribute to the search for point sources in the northern sky at least for energies above 10^{15} eV with competitive quality.

5. The central detector

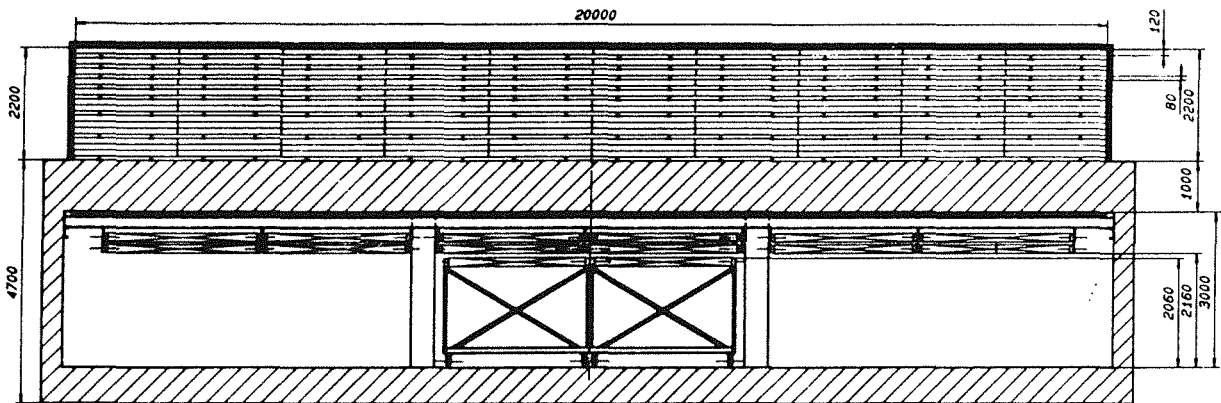


Fig.5.1 Schematic cross-section of the central detector.

The fundamental design goal of the central detector is to provide particle detection in the shower core with the following properties:

- Identification and energy measurement for hadrons from 10 GeV to 10 TeV with sufficient precision.
- Separation of individual hadrons by a fine grain spatial segmentation.
- Effective separation of the soft and hard components.
- Measurement of the muon component at the bottom of the calorimeter.

After discussing the physical, technical and economical aspects of various possibilities of realization [58], the following concept emerged. The main component of the detector consists of an iron calorimeter with lateral dimensions of 16x20 m² and a longitudinal depth of 2.2 m. A schematic sketch of the lay-out is shown in Fig.5.1, indicating also the basement where the chambers for muon detection will be installed.

5.1 Absorber

The absorber thickness varies, beginning with thin layers of less than one interaction length λ_0 in the upper part to thick layers of $2.5 \lambda_0$ at the bottom. The total thickness corresponds to $11 \lambda_0$. This ensures that low energy hadrons of approximately 10 GeV as well as high energy hadrons of up to more than 10 TeV can be well recognized and measured with a nearly constant energy resolution of 35%.

The absorption layers will be built up of slightly radioactive iron. This iron is available from a dismantled reactor station and other sources within KfK. An activity of up to 10 Bq/g can be tolerated. The use of iron instead of concrete has the advantage that electromagnetic showers develop faster than hadronic showers and therefore the soft component can be reasonably well separated without a lead filter above the calorimeter.

Electrons are absorbed up to 95% in a layer of 10 radiation lengths X_0 . From tab. 1 it can be inferred that this length corresponds to one interaction length λ_0 in iron. In a lead filter, of course, electromagnetic and hadronic energy would be even less mixed. Operating experience has to show, whether an additional filter of 5 cm lead will be necessary.

Tab. 5.1 Radiation length X_0 and interaction length λ_0 .

	Concrete	Iron	Lead
$X_0(\text{cm})$	10.7	1.76	0.56
$\lambda_0(\text{cm})$	40.0	16.7	17.0
$10X_0/\lambda_0$	2.5	1.0	0.3

5.2 Active layers

In between the absorber slabs active elements are introduced to sample the deposited energy. Liquid ionization chambers are chosen because they are the most preferable choice for good calorimetry for the following reasons:

- Signal proportional to energy deposition, and no saturation in dense cores.
- Absolute calibration by charge injection possible.
- Long term stability due to feed-back amplification.
- Large dynamic range.
- Signal independent of position, no edge effects.

The first four properties are especially important for a calorimeter as considered here. With showers in the TeV energy range high ionization densities have to be measured which spread up to 3 orders of magnitude. Due to shower fluctuations even 4 orders are encountered in practice. Since the calorimeter cannot be calibrated in a particle beam above a few hundred GeV, we have to rely on the energy deposition simulated by Monte Carlo codes and on an absolute calibration of the ionization chamber. In an ionization chamber the charge is collected without being amplified. Electronic amplification of the signal is feed-back controlled, thus ensuring a stable operation even over years.

The chambers will be flat stainless steel containers of lateral dimensions 50 x 50 cm² and 1 cm thickness as sketched in fig.5.2. The inner electrode has a potential of 5 kV and is segmented into 25 x 25 cm² pads, which are read out separately. In this way individual hadrons can be distinguished and their energy measured. The number of electronic channels, however, is quite large. For eight instrumented layers 40000 channels are necessary.

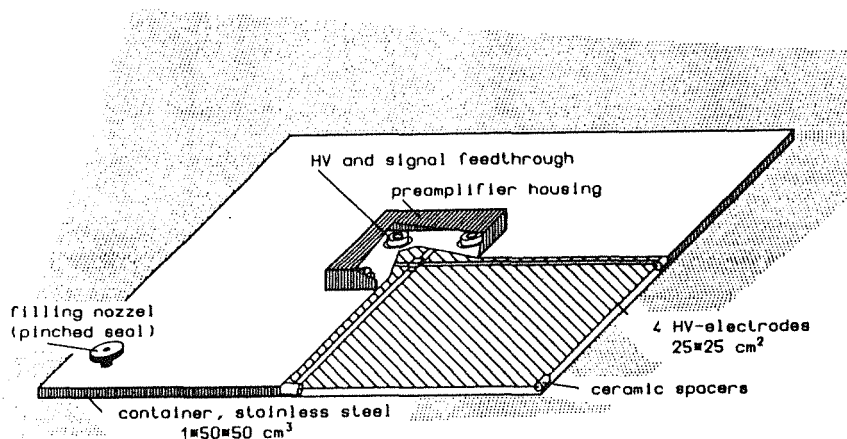


Fig.5.2 Sketch of a liquid ionization chamber.

It is planned to use tetramethylsilane TMS ($\text{Si}(\text{CH}_3)_4$) and hexamethyldisilane HMDS ($\text{Si}_2(\text{CH}_3)_6$) as ionization liquids. A mixture of approximately 4 : 1 will probably represent a good compromise between the requirements of a large and fast signal on one side and safety requirements on the other side. Among the

dielectric liquids at room temperature TMS shows the best electron conduction and is commercially available at a reasonable price. However it has a high vapour pressure causing problems at temperatures above 27°C. An admixture of HMDS lowers the vapour pressure without destroying the good conductivity for free electrons. Chambers with TMS have been developed in the institute since 1984 [59]. Experience with the new type of flat chambers is described in sect. 5.6.

5.3 Muon chambers

At the bottom of the calorimeter muon chambers are mounted below the ceiling of the basement. The calorimeter absorbs muons up to 2 GeV. All muons of higher energy penetrate the calorimeter and are detected in the chambers. Their anode wires are typically 2 m long and separated by 13 mm. Correlated space points are obtained by read-out of cathode strips oriented $\pm 34^\circ$ with respect to the anode wires. The spatial resolution in both directions is $\sigma = 6$ mm. The operation gas is a mixture of 2/3 argon and 1/3 isobutane.

The chambers have been taken over from CEA/CEN Saclay and have been used as muon detectors in the CELLO experiment. They cover an area of 300 m² and are described in detail in [60].

5.4 Trigger counters

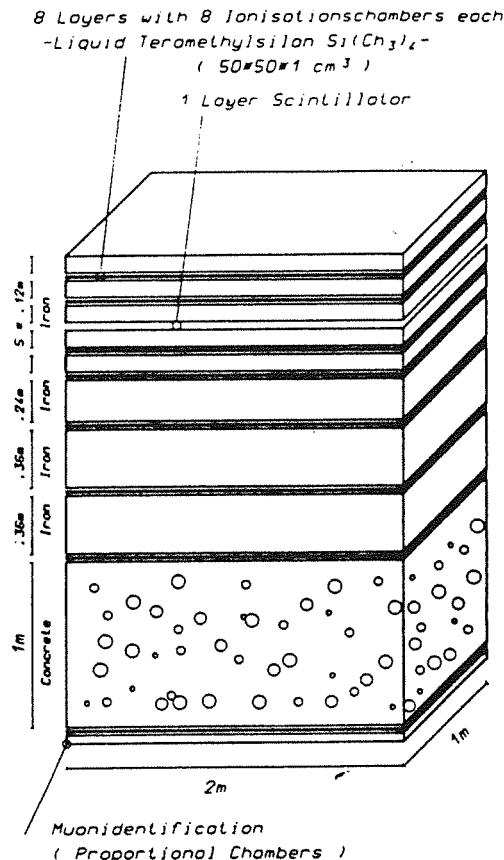


Fig.5.3 Vertical structure of the central detector.

Behind the 3rd iron plate, at $1.9 \lambda_0$ (the maximum of the shower development) a gap is left for a fast trigger layer of plastic scintillators. At the shower maximum they will be sensitive only to hadrons and will serve two purposes: a) to measure the arrival time of the hadronic particles, and b) to deliver a fast trigger signal for the ionization chambers und muon counters.

The vertical structure of the central detector as described above is shown in more detail in fig.5.3.

5.5 Simulated calorimeter performance

The response of the calorimeter to incoming hadrons has been simulated using the program SCHEME, which is a frame containing several codes. For hadronic particles it uses the codes GHEISHA, HETC and MORSE and for electromagnetic particles the code EGS4 [61].

As an example the deposited hadronic energy of a 10^{15} eV air shower is shown in fig.5.4 as seen in the calorimeter from the top. A total of 150 hadrons hit the central detector. They deposit an energy of 4 TeV, out of which 21 GeV are detected in the active layers.

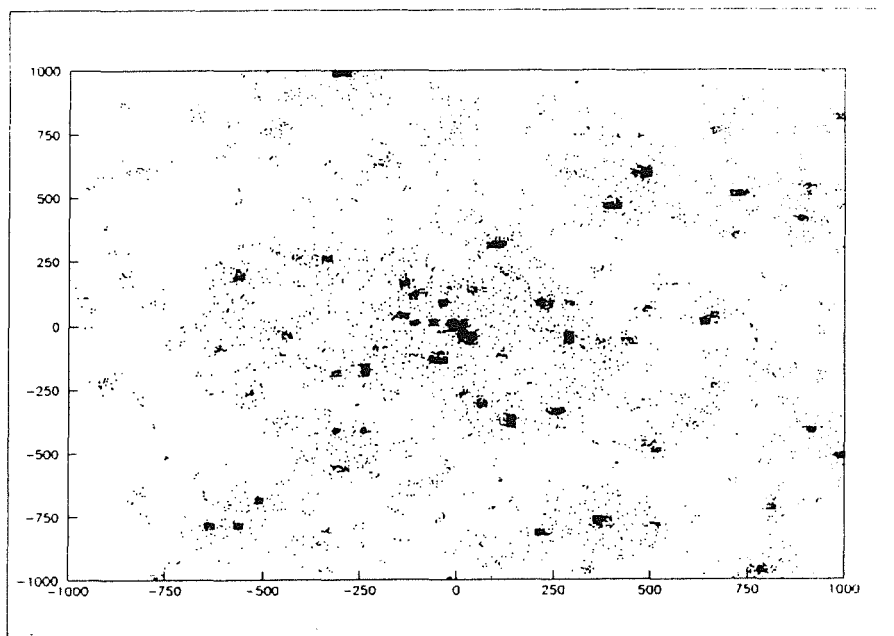


Fig.5.4 Scatter plot of the hadron energy deposited by a 10^{15} eV air shower in the central detector.

The energy resolution for incoming pions is shown in fig.5.5. In the calculations GHEISHA was used for the high energy part. Below 1 GeV they are followed by HETC and neutrons below 20 MeV by MORSE. One observes that in the energy

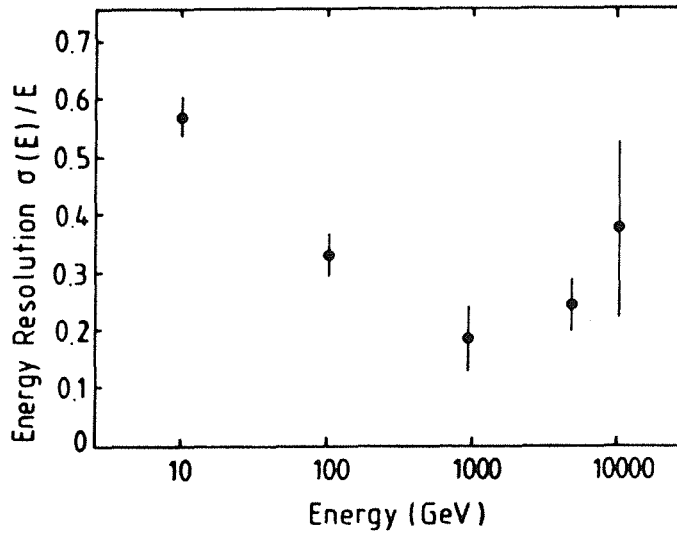


Fig.5.5 Energy resolution of the calorimeter versus primary energy (M.C.results).

range from 10 GeV to 10 TeV the calorimeter exhibits a mean energy resolution of $\sigma(E)/E \approx 35\%$.

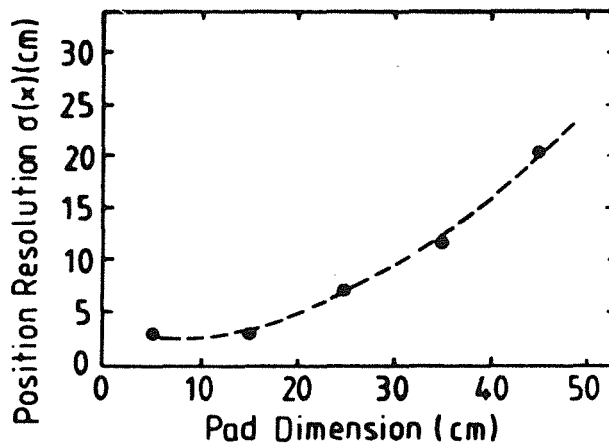


Fig.5.6 Accuracy of determining the central position of a hadron shower for different pad sizes of the ionization chambers.

Fig. 5.6 demonstrates the accuracy which can be obtained in locating hadrons by weighting the energy in individual pads. For showers of 10 GeV pions the resolution is shown with respect to varying segmentation. It is obvious that with the pad size of $25 \times 25 \text{ cm}^2$ a reasonably good determination of the shower position of $\sigma(x) \approx 8 \text{ cm}$ can be achieved. This accuracy is widely independent of the shower energy and does not change essentially up to the highest energies.

Another interesting parameter is the position of the maximum of the cascade in the calorimeter which can be inferred from the transition curves in fig.5.7. One

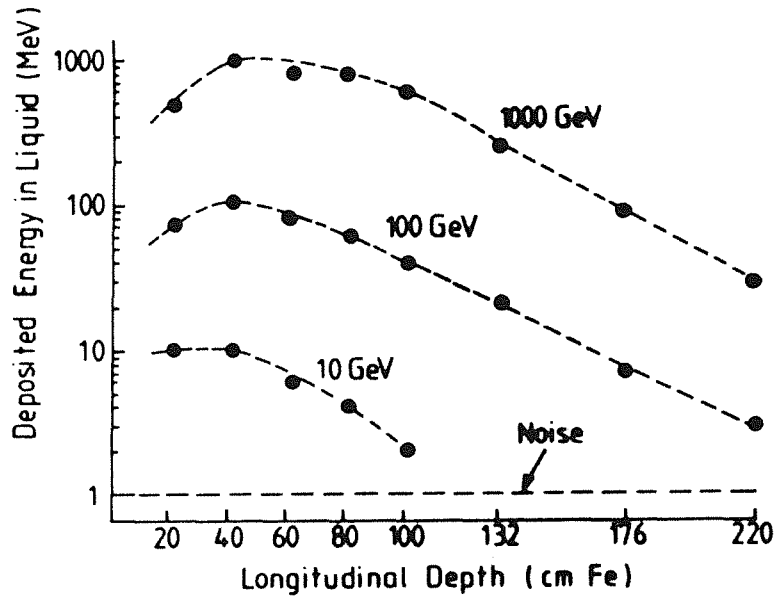


Fig.5.7 Transition curves for pions of 10, 100 and 1000 GeV.

notices that this position does not change drastically with energy. The trigger counters will be placed as near to the mean maximum as possible, i.e. at $1.9 \lambda_0$ or after the 3rd iron slab. Fig. 5.7 also shows the level corresponding to the preamplifier noise. 10 GeV is the envisaged energy threshold for hadron recognition. As can be seen, the energy deposition at this energy is well above the electronic noise level and hadrons will be easily recognized as such.

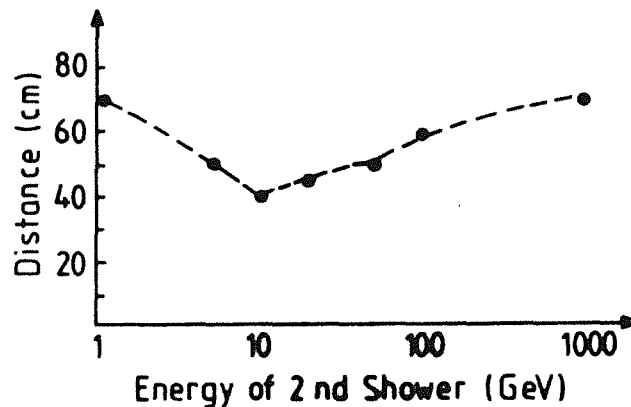


Fig.5.8 Minimum distance between two resolved showers; one shower is assumed to have a fixed energy of 10 GeV, and the second is varying in energy.

An idea of how well nearby showers can be separated from each other is shown in fig. 5.8. Plotted is the distance of two showers which do not overlap by more than

20 % in energy deposition. One of the showers has a fixed energy of 10 GeV, whereas the energy of the second is varied. One notices that the best separation is obtained when both showers have equal energy. The mean separation of 50 to 60 cm ensures that the number of hadrons can be counted in nearly all cases except for the dense cores in high energy showers, where we will measure only the sum of hadronic energy.

5.6 Ionization chamber performance

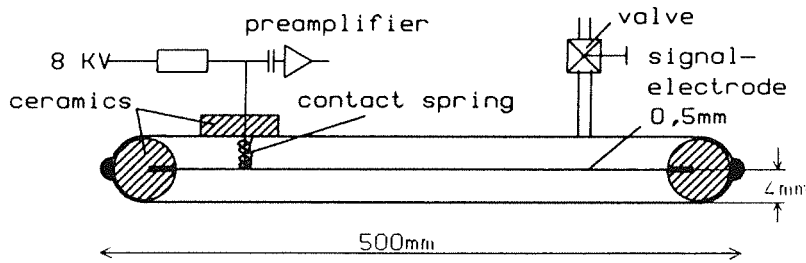


Fig.5.9 Principle of the chamber lay-out.

The principle of the chambers are shown schematically in fig.5.9. The stainless steel container is formed by welding together two halves along the 4 edges vacuum tight. The central electrode is positioned by ceramic spacers, giving a gap of 3.5 mm on both sides. The chamber contains 1.7 litres of liquid. A nozzle serves for pumping and filling and is pinched tight after complete filling with a steel clamp. A voltage of 5 kV is needed to achieve a field of more than 15 kV/cm. The signal is picked up by a spring which connects the electrode with a ceramic insulator feed-through from where it is capacitively coupled to the preamplifier.

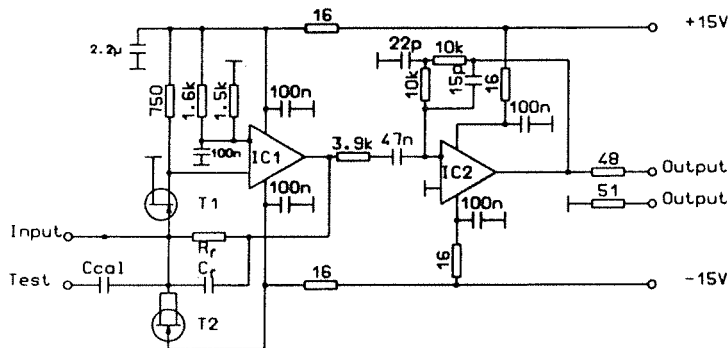


Fig. 5.10 Diagram of the amplifier input circuit.

A schematic diagram of the amplifier input circuit is shown in fig. 5.10. Two inputs are provided to each channel: one from the chamber electrode, and one

capacitively coupled from the calibration line. The coupling capacitor will be as small as possible, typically 2.2 pF. The total capacitive load at the input is 500 pF. Hence, for T₁ a FET with a high input capacity will be chosen, typically SK371. After being processed by the integrating and differentiating circuit IC2, the signals are transmitted to a main amplifier which is located in the central acquisition room. A bipolar shaping with a time constant of 1µs is used. The following signal digitization is shown schematically in fig. 5.11. The analog pulse is stored in a sample and hold circuit and compared with a central stair-cause function. The latter is generated for 4000 channels in parallel.

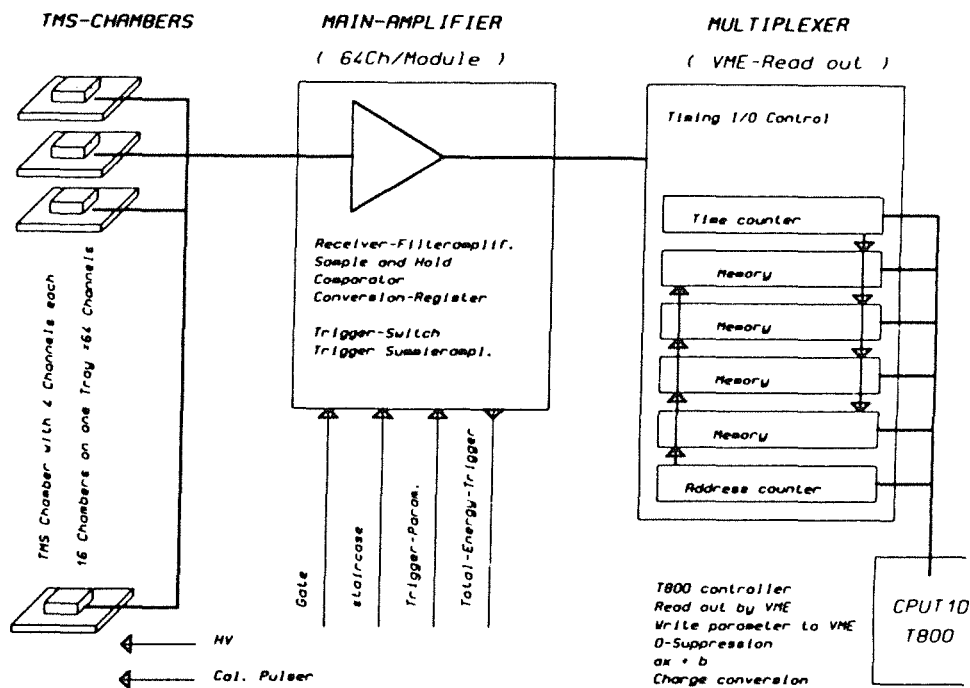


Fig. 5.11 Scheme of electronic pulse handling.

A critical part when finishing the chamber is the cleaning procedure. For obtaining a high purity the chamber is constructed only from ceramic and stainless steel. All plastic components have been avoided. The usual cleaning method of baking in a vacuum at reasonably high temperatures around 700 - 800°C is not applicable for chambers in mass production. Therefore, a faster procedure which allows easier handling has been developed. It consists of a chemical cleaning by etching, an ultrasonic bath in ethanol and ultra pure water (volume resistivity ~ 18.3 MΩ cm). After finally being assembled the chamber is purged under glow discharge. For this purpose the chamber is filled with a mixture of argon and 5 % O₂ at ≈ 10 Pa and a dc-voltage of 300 V is applied to the inner electrode. Reaction products like CO, CH₄, H₂O and CO₂ are pumped away. After a few hours of treatment the chamber is clean enough to be filled, and is

flushed three times with clean TMS in a fast manner in order to rinse away all dust particles.

The TMS used has an impurity level of less than 10 ppb O₂ equivalent. After flushing with this liquid one or two times within approximately 24 hours, the liquid stays in the chamber with an impurity concentration below 20 ppb. At a field of 15 kV/cm this ensures a signal loss of not more than 3 %. No experience in long term behaviour of these chambers in their final version with a pinched-off seal and without any plastic construction parts exist at the time of writing. From measurements with other chambers containing some organic material we can deduce that the signal loss should be less than 10%/a. At CERN a group [62] has operated a similar device for 14 months without any noticeable signal diminuation.

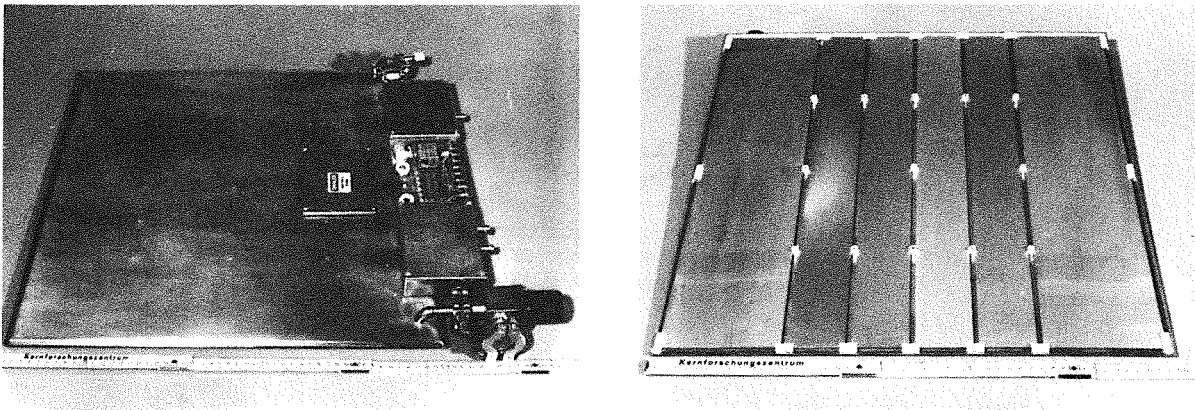


Fig.5.12 Test chamber with preamplifier boxes (a), the chamber open (b).

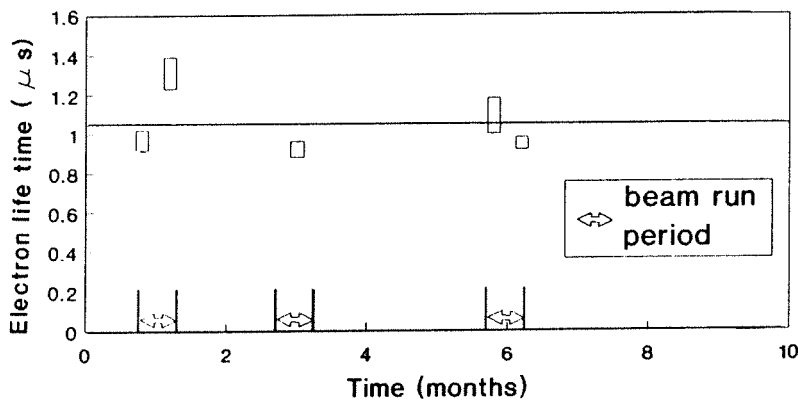


Fig.5.13 Life time of free ionization electrons in a prototype chamber with respect to the time elapsed since closure.

Two chambers were tested with an accelerator beam consisting of pions, electrons and muons. A photograph of a test chamber is shown in fig.5.12. The measurement was performed at the ITEP institute in Moscow in a 6 GeV beam line.

The chambers exhibit a very constant signal response as is demonstrated by fig. 5.13. The life time of free ionization electrons did not decrease within 8 months, although the chambers were closed with a valve using a viton gasket.

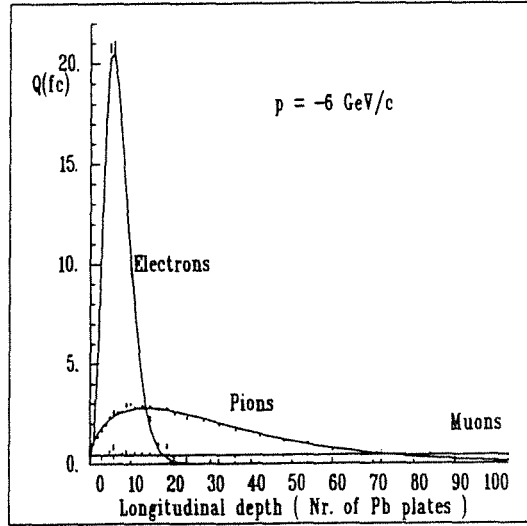


Fig.5.14 Transition curves for 6 GeV particles in Pb as measured with a TMS ionization chamber.

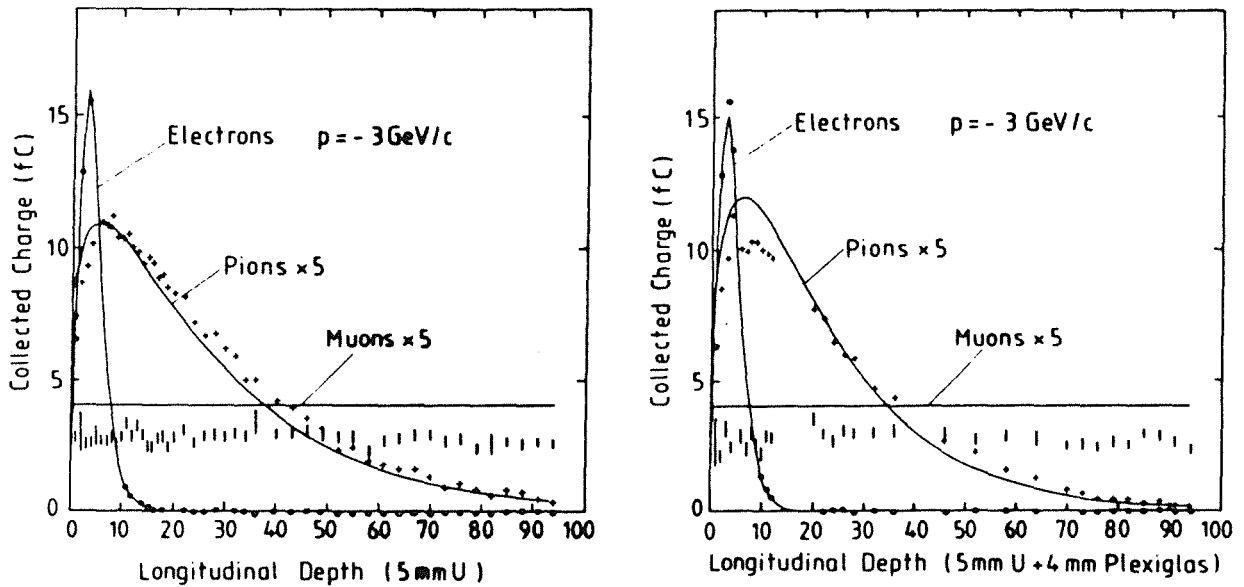


Fig.5.15(a) Transition curves of 3 GeV particles in U compared with M.C. simulations. (b) same as (a) but U plates interleaved with plexiglas.

Results are given in fig.5.14. The cascade development in lead is plotted for three different particle types of 6 GeV. It shows the distinct behaviour of the transition curves. A closer look is given in fig.5.15 where the measurements at 3 GeV are compared with shower simulations by M.C. codes. One observes that the measured transition curve for electrons coincides well with the EGS4 calculation. This proves that the chamber calibration is correct. For pions, however, we observe deviations as well as for muons. Because we have to rely at high energies on M.C. codes when calibrating the energy scale in the TeV range, a thorough study is mandatory. Test measurements at higher energies up to 300 GeV are foreseen.

5.7 Muon burst counters

The muon chambers in the basement detect all muons above 2 GeV. Very interesting, however, are muons above 100 GeV because they originate predominantly from the first interactions at the top of the atmosphere. Their energy should be measured, at least approximately. In a later extension of the experiment this could be done by using the electromagnetic radiation such as bremsstrahlung and direct pair production of these energetic muons. The critical energy for muons in lead is 180 GeV and 350 GeV in iron. For muons direct pair production dominates bremsstrahlung by 50%, and it is a softer process, i.e. the pairs produced have low energies, namely about 2% of the parent muon. The energy loss by pair production does not fluctuate as much as that caused by bremsstrahlung and can be used to determine the primary energy roughly [63]. A concept for such

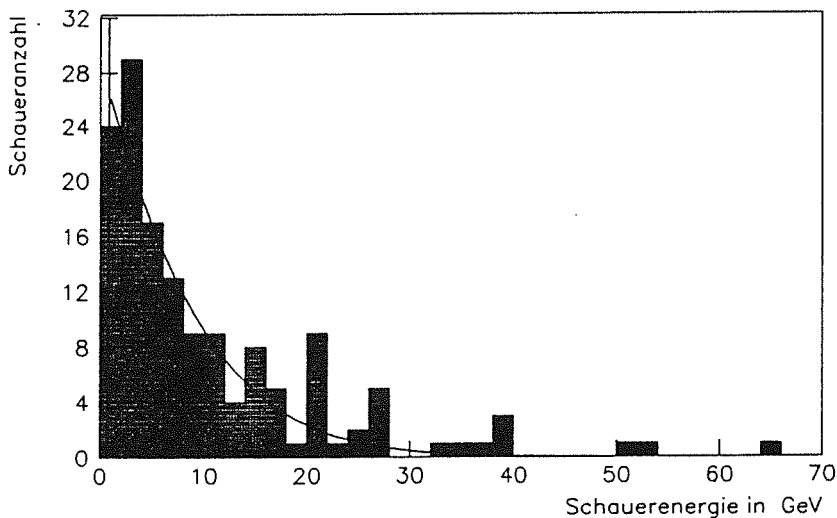


Fig.5.16 Energy deposited by horizontal muons in an uranium calorimeter.

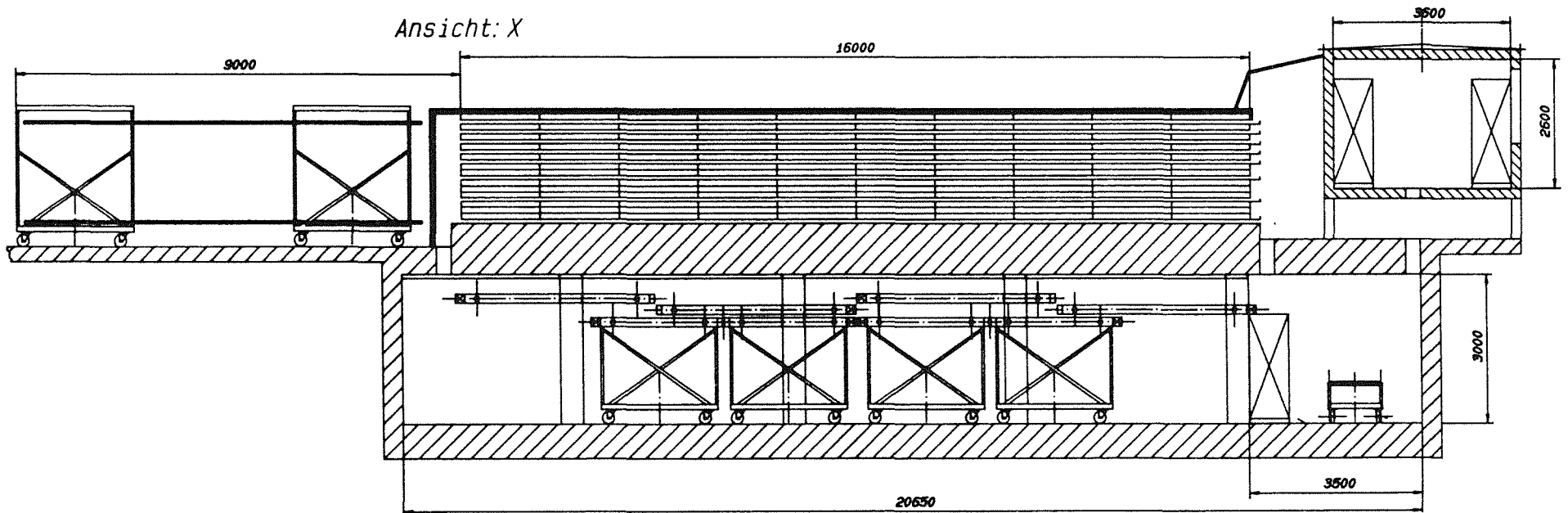


Fig. 5.17 General view of the central detector with charging facility and central data acquisition room.

a 'burst' counter consists of a stack of lead plates interleaved with ionization chambers. For a stack of 20 cm Pb an energy resolution of 40% for muons with energy more than 300 GeV can be estimated.

Prototypes of such burst counters using depleted uranium and lead as radiator plates are under test. The energy radiated by horizontal muons as measured in such a calorimeter is reproduced in fig.5.16.

5.8 Installation

The central detector is of modular design. The iron slabs have the dimensions 1.6 x 2.5 x 0.12 m³. They are stacked on a concrete basement, the ceiling of which serves as the last absorber layer. Free space between the iron layers is kept by iron T-bars. The very last layer of ionization chambers will be mounted below the ceiling just above the muon chambers.

The ionization chambers will be introduced into the empty gaps on long trays from one side as indicated in fig.5.17. A charging facility for this purpose is indicated in fig. 5.17. The cables will come out on the side of the electronics hut. The basement is shown to be below ground level. It also takes all the power supplies for low and high voltages and the gas supply for the muon chambers.

6. Data acquisition, processing and storage

The most difficult task of data acquisition and storage in the KASCADE experiment arises from the requirement that all detector signals originating from a true air shower event should be registered including their relative timing whereas uncorrelated signals should be widely suppressed. These uncorrelated signals occur at a rate of several hundreds per second in each detector channel as compared to a true event rate of about one per second in the whole array. Yet data acquisition should have negligible dead time and on-line suppression should not lead to accidental suppression or incomplete read-out of true shower signals in order to preserve the best statistics possible for the shower size measurement. Hence, it is preferable to store a few uncorrelated data which are rejected later by off-line analysis. According to the spatial extension of the KASCADE array true air shower events are expected to be correlated within below 1 μ s.

Another important task of data acquisition which influences the method of background suppression is the required high precision of the relative time measurement between the detectors in a cluster. This is needed for the determination of the shower direction and of the relative arrival times of different shower components.

With regard to these aspects fast on-line suppression of uncorrelated signals and selection of true data is performed by a method which uses hardware processes as well as software procedures.

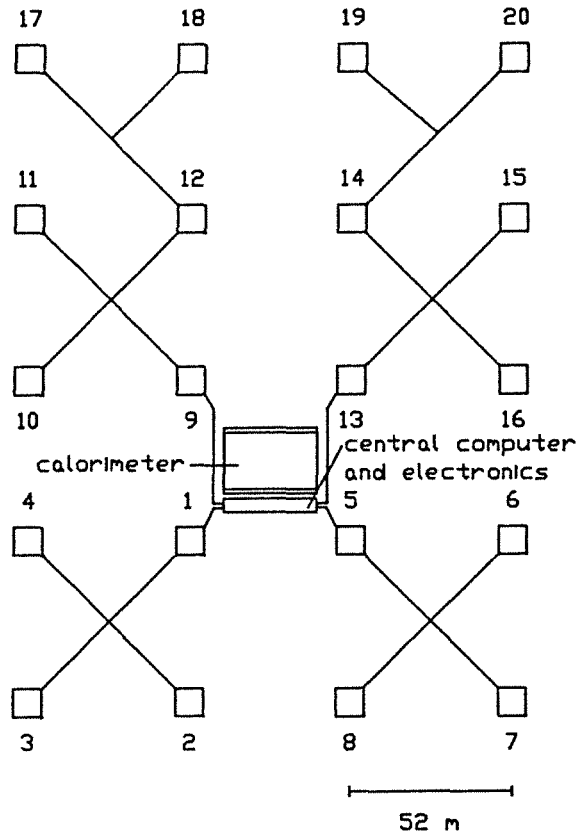


Fig. 6.1 Location of the cluster electronics and computers in the array and at the calorimeter and planned connections. The distances between the array computers and the calorimeter as well as the size of the latter are to scale.

Besides the front-end electronics of the array clusters and of the central calorimeter the main hardware components of the data acquisition system are:

- fast hardware event triggers
- a 5 Mc (200 ns) clock ('micro-time') on a common synchronized time bus available in each of the clusters, at the central detector electronics, and at the central data acquisition computer

- a subnanosecond TDC ('nano-time') in each electron/photon detector channel
- a powerful micro-processor in each of the clusters and several of such micro-processors responsible for calorimeter read out
- a central computer for data handling and storage to which all of the micro-processors are linked by fast data lines

In addition, a rubidium oscillator in connection with a DCF 77 radio clock is used for absolute time measurement (UTC). The accuracy of absolute time is expected to be of the order of 1 μ s for each event. The location of the array electronics and micro-processors, the connection of the latter with the central computer, and the distances to be bridged are indicated in fig. 6.1.

6.1 Event trigger and selection of data

The general principle of the event trigger in the array and selection of data can be characterized as follows:

- A 'true event' trigger is generated by electron/photon detectors only.
- No main hardware event trigger for the whole array exists.
- Instead, fast triggers are generated independently in each array cluster and in the central calorimeter according to requirements given below.
- Signals from different clusters and from the central detector belonging to the same air shower event are identified off-line by an arrival time label (micro-time), which is attached to the amplitude signal of each individual detector channel.

For the detailed discussion of the triggering mode, we first concentrate on the array only.

The front-end electronics for one channel of the electron/photon detectors in the array clusters is shown schematically in fig. 6.2. The corresponding electronics for the muon counters in the array (version with scintillation counters, see sect. 4.4) is quite similar, however without the TDC-branch. The total electronics and read out for a whole cluster will fit into a single VMEbus crate together with the local micro-processor which also serves as crate controller.

As soon as an input signal from the PM tube exceeds a given threshold of the input discriminator

- the counter of the micro-time clock is read into a register,
- the TDC of 200 ns width (8 bit resolution) is started,

(dualport RAM) which assigns 'not empty' to the local processor through a flag. Because of the 16 bit range of the micro-time counter it has to be reset every 10 ms. In order to avoid ambiguities in the data an additional toggle bit is assigned to the data words which is switched when the micro-time counter is reset. Hence, also such events are correctly recognized which occur close to the reset of the micro-time counter. For the nano-time measurement some special hardware treatment is also necessary if the start pulse for the TDC occurs very close to the next stop pulse. The next but one pulse is taken in this case to preserve reliable time measurement.

In case of too low particle density in the cluster the data processing will be cancelled by a veto signal before transfer to the FIFO memory in order to keep the required memory size small and to prevent excessive dead time from background. The veto signal is enabled if less than 5 out of the 64 detectors fire.

Signals from the muon detectors in the array are treated in a different way. Since the intensity of the electron/photon component drops steeper with increasing distance from the shower core than that of muons the former may be too weak in outer regions of the shower to exceed the coincidence conditions. Yet the muons should be registered in this region. Therefore signals from the muon detectors are always digitized and stored in the FIFO, independently of the existence of a 'true event' trigger.

The FIFO memories are successively scanned in the daisy chain cycle and their contents is buffered in the memory of the local processor. Read out of one FIFO memory will take less than 1 μ s so that the full scanning cycle of a cluster lasts about 300 μ s.

Further processing of these prestored data is controlled as follows: Whenever the 'true event' signal reaches the central computer a command is forwarded from here to each of the cluster processors. It is then checked whether their memories contain signals with a micro-time mark close to the trigger depending on the distance between the clusters and on the estimated shower direction. (This estimate can be made locally in the cluster computer after FIFO read-out.) Due to the fast data links between the central and local computers (see below) the command may reach the cluster processors before the corresponding FIFO scan has been finished so that the prestored data are processed immediately.

True event data selected this way are finally transferred to the central computer where they are further processed and stored together with the absolute time (UTC) from the rubidium oscillator. Uncorrelated data in the local memories are erased after due time.

Summarizing the method of event triggering and selection of valid data it should be noted that conversion of analog signals, and of nano-time on one hand and processing of event trigger and read-out commands on the other are done *in parallel*. By this procedure, by the local event recognition on cluster basis, and by the decentralized selection of data the array works essentially without dead time. The uncorrelated background of about 250 counts per second in each channel is negligible when compared to a total processing time of few μs .

6.2 Trigger for the hadron calorimeter

The ionization chambers in the central calorimeter provide signals which are much too slow for a fast event triggering and timing. In addition, AD conversion of the calorimeter signals takes about 1 ms due to the large number of channels and the need for multiplexing (see below). Therefore, special attention has to be paid to the triggering of the calorimeter. In particular, conversion and processing must be started only if a true event has definitely been recognized.

For this special triggering purpose the central hadron calorimeter contains a layer of scintillation counters as discussed in sect. 5.4. These counters are equipped with front-end electronics very similar to that of the array electron/photon detectors (see fig. 6.2) with the exception that an 8 bit resolution is sufficient for the nano-time. The scintillators are segmented into about 150 independent units which are controlled by at least 2 micro-processors being equivalent to 2 clusters from the data acquisition point of view.

In addition to these scintillators the four clusters surrounding the central detector fulfill a special task in triggering it. Direct lines of their 'true event' signals are fed also to the electronics of the central detector.

Two cases of events and correspondingly of trigger modes are distinguished. In the first case the shower core does not hit the calorimeter but is located far away in the outer region of the array. Only for energies above a few 10^{15} eV the particle density in the central clusters will be high enough in this case to fulfill the usual 'true event' condition. The ionization chambers and muon chambers should nevertheless be triggered for muon detection.

Identification of correlated muons is provided in this case by a coincidence circuit between the scintillator segments on one hand and the muon chambers on the other as indicated in fig. 6.3. Whenever such a muon burst is detected its micro-time from the scintillator is processed in the same manner as in the array. The corresponding micro-processors buffering these events are read out from the main computer when a 'true event' was announced from an array cluster.

In the second case in which the shower core hits the calorimeter or close to it the particle density in all four of the neighbouring array clusters is high enough to fulfill the usual 'true event' condition. This signal in coincidence with a signal from the calorimeter trigger plane provides the direct master trigger for the ionization chambers and muon chambers beneath. The scintillator layer in the calorimeter encounters a high particle density mainly due to hadronic showers produced in the iron absorber. These signals are used to measure the arrival time of hadrons with respect to the electron/photon component in the array detectors with the same technique as used to measure the relative times in the array (i. e. no additional hardware coincidence conditions are needed). Besides initiating AD conversion and full data processing in the calorimeter and muon chambers the trigger signal from the neighbouring array clusters also initiates the command from the central computer to the local systems to read out the data of the ionization chambers and muon chambers.

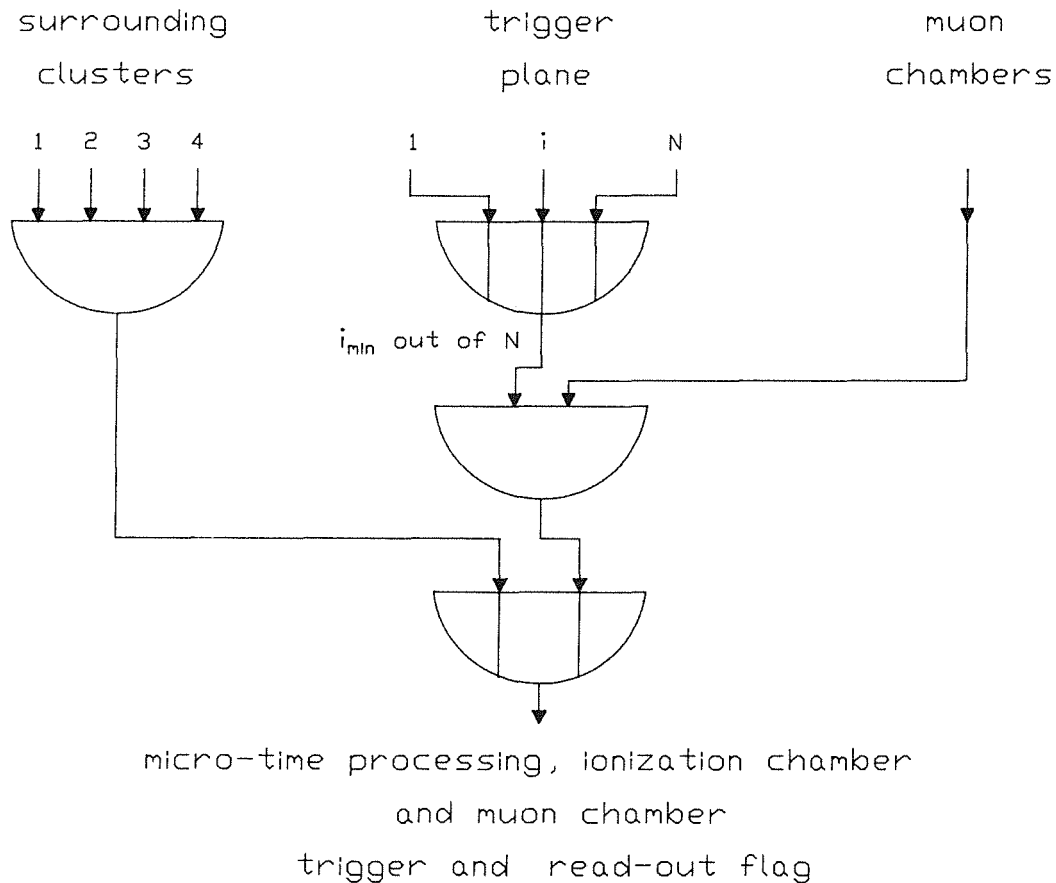


Fig. 6.3 Hardware trigger for the ionization chambers and muon chambers of the central detector.

6.3. Calorimeter data processing

The ionization chamber signals are stored in a sample-and-hold circuit on the main amplifier card and compared with a staircase voltage which is common to all channels (see fig. 5.12). The conversion has a double slope characteristic in order to obtain a sufficient resolution for the small energy deposited by a penetrating muon as well as for the high density of ionization in a shower core. Muons deposit typically 1 to 3 MeV in a chamber, depending on their momentum and direction. On the other hand an energy loss of 1000 MeV has to be encountered for a 1 TeV shower. The conversion slope, therefore, will increase by a factor of 16 for the upper half of the ADC range. The data will be stored in a 13 bit register. For generating the reference voltage a 13 bit DAC will be used.

The common staircase voltage has a step length of 1 μ s. During this period the signals of 16 channels are compared serially and the data are transmitted to the multiplexer (see below). Conversion to a 13 bit word thus takes approximately 1 ms. The organisation of the conversion and data handling prior to read-out is done on a multiplexer card in a VME crate (see fig. 5.12). The channels are read out into T800 transputers which perform first data filtering, i.e. processes like zero suppression, voltage to charge conversion, and pattern recognition. The T800 also control the stability of the electronics and the calibration of the amplifiers by charge injection at the preamplifier input.

The read-out of the muon chambers is described in ref. [61].

6.4 Local and central data acquisition computers

The described data acquisition concept takes advantage of the properties of the special micro-processors. These are INMOS T800 transputers which have also been applied successfully in the dedicated computer for shower simulations (see sect. 3.3.1). One advantage of these micro-processors for the present application is that they do not need a disk operating system. The user software can be loaded directly from a host computer which runs under a widely used operation system such as UNIX. Hence, delicate mechanical disks are not required in the cluster stations.

Another important characteristics of the transputers is of particular advantage for the experiment, namely the existence of 4 fast serial data links which can transmit up to 20 Mbit per second in both directions. Moreover, data transmission via these links does not influence the operating speed of the powerful 32 bit

central processor and its access to the on-chip floating point unit and 4 kbyte internal memory.

The links consist of 2 lines each, one for each direction. One is used for the forwarded signal (8 usable plus 3 control bits) and the other for the 'acknowledge' signal which must arrive from the partner before the next data word is transmitted. The link connections are designed for short transmission distances only. With the use of opto-couplers, however, these distances may be considerably increased. According to the simple transmission protocol described above the transmission rate decreases for distances larger than 100 m. Nevertheless, even with rather cheap opto-couplers which allow rates of 5 Mbit/s only the data transfer rates are about 0.2 Mbyte/s on the longest distance in the array.

Data transfer via transputer links means that the only connections between the cluster stations and the central computer consist of 2 fiber optics strings.

However, the method works successfully only if sufficient transputer links are available also in the central computer. Hence, its main computational power will also consist of transputers in an architecture shown schematically in fig. 6.4.

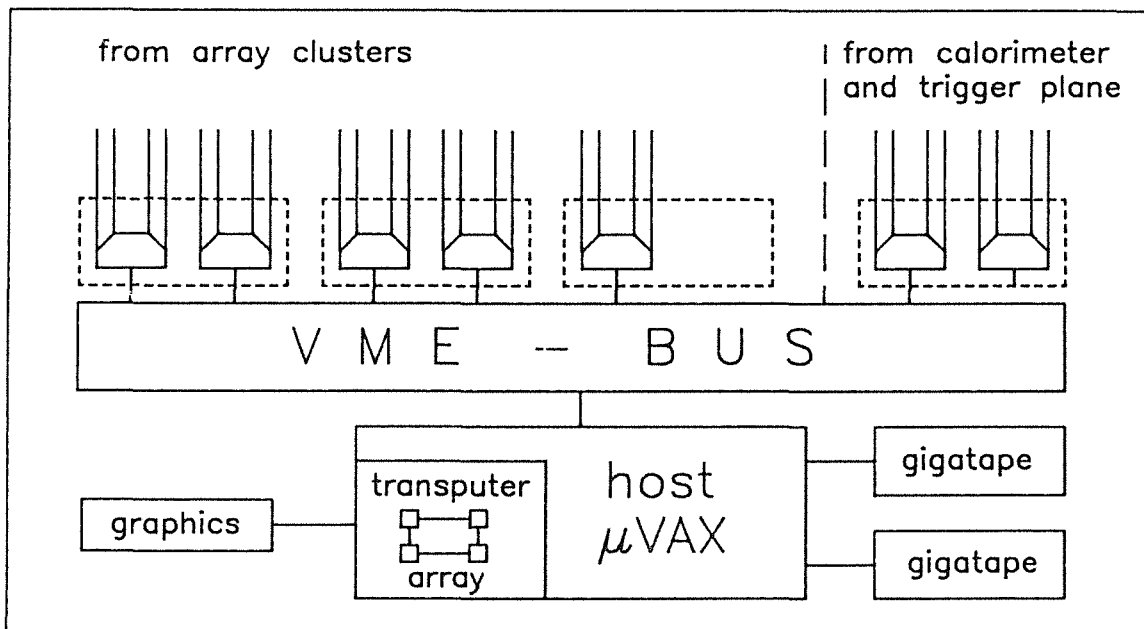


Fig. 6.4 Architecture of the central data acquisition and processing computer and its connection to the peripheral processors (schematically).

The host computer is assumed to be a workstation with peripheral equipment such as hard disks and tapes for soft-ware back-up and optical disks for the air shower data. The number of transputers is not fixed so far. The example in fig. 6.4 shows 8 processors in the central computer each of which is connected to another 4 in the array and calorimeter read out. (The latter is assumed to need 5 local processors

for the ionisation chambers and additionally 1 for the muon chambers). Slightly different configurations are also possible. For online processing a number of additional transputers (4 in the example of fig. 6.4) are adopted to the central data acquisition computer. The number can easily be increased according to the on-line processing requirements, and link connections between the processors are possible to form a parallel computer.

The data rates to be processed by the central computer are dominated by the rate of air showers at the low-energy threshold of the experiment (ca. $3 \cdot 10^{14}$). This rate is about 1 - 2 /s. After zero suppression 4 kByte / s are expected from the detector array, 5 kByte /s from the muon chambers in the central detector and additionally 2.5 kByte /s if liquid ionisation chambers are readout in order to improve the muon track reconstruction. Hence the total rate is expected to be 10 - 12 kByte /s.

7. Other comparable experimental installations

KASCADE is characterized by the following features:

- The three main components of an extensive air shower, i. e. electrons and photons, muons, and hadrons, are registered for each individual event and
- the degree of sampling is so high that the scatter of the observable quantities are governed by the intrinsic fluctuations of shower development rather than by the limited detector area.

We know of no other experiment operational today which achieves similar accuracy in these respects. For some of the larger air shower experiments this will be discussed in more detail in the subsequent paragraphs.

7.1 Experiments including large hadron calorimeters.

To the best of our knowledge there are at present four air shower experiments operational or under construction which employ larger hadron calorimeters, those at Akeno, Tien Shan, Gran Sasso, and the ANI installation on Mount Aragats. All three are situated well above sea level at between 900 and 3250 m of altitude.

7.1.1 The Akeno experiment

This experiment is situated ca. 100 km west of Tokyo at a height of 900 m above sea level. It was started approximately 25 years ago and its first stage included 169 m² of scintillation counters for electromagnetic particles, 300 m² of muon counters, and a 100 m² hadron calorimeter on a total area of 1 km² [64]. It has recently been expanded to 20 km² [65], and a further expansion to 100 km² is

under way [66]. As shown by this development, the emphasis of the present work with the Akeno array is on the investigation of cosmic rays at the highest energies, a field to which the Akeno group have made substantial contributions [67].

The array part of the original 1 km² Akeno installation represents a detector coverage of 0.0169 % for the electromagnetic component and of 0.03 % for muons. At this level the sampling will determine the fluctuations of the measured electron and muon numbers completely. In the energy range of the KASCADE experiment a sampling fraction of approximately 1 % is required in order to reduce the sampling fluctuations to the level of the intrinsic ones according to our simulation calculations. The sampling rate of the extended installations is considerably lower than that of the 1 km² array. Since the electron to muon ratio is the shower observable most sensitive to the mass of the primary this implies that it will probably be very difficult to obtain information about the primary mass composition with this installation. The experiments aim, in fact, at determining the primary energy spectrum at the highest energies.

The calorimeter or 'energy flow detector' [68], as it is called, has a size of 10x10 m² and employs 5 layers of proportional chambers below different depths of concrete. The topmost layer is unshielded. The other four are placed under total depths of 0.5, 1.0, 1.5, and 2.75 m. The spatial resolution is 10 cm in one dimension [64]. Only one coordinate can be registered in each layer. In view of the large particle density in the shower core it will be very difficult, to say the least, to identify individual hadrons and measure their energy. The small number of sensitive layers and the limited thickness which results in a considerable leakage at the lower end of the concrete absorbers lead to an energy resolution which we estimate to be not better than a factor of two. It is obvious that the KASCADE calorimeter will represent a considerable improvement in this respect.

7.1.2 The Tien Shan experiment

This experiment is located in the Tien Shan mountains at an altitude of 3340 m above sea level. It consists of a somewhat irregular array of ca. 70 m² of scintillation counters and about half this area of Geiger-Müller counters, both distributed up to 180 m from the central station [69]. The sampling of the electromagnetic component in the central part of the experiment, a circle of 40 m diameter, amounts to ca. 0.5 %.

The original setup [70] contained a calorimeter consisting of 14 layers of ionization chambers separated by lead layers 2.5 or 5 cm thick. The total thickness

of approximately 75 cm corresponds to ca. 4 interaction lengths. The active elements are ionization chambers of $5.5 \times 11 \times 300 \text{ cm}^3$ filled with argon plus 5 % of nitrogen. Each layer comprises 96 of these chambers. The long axes of the counters are oriented at right angles in adjacent layers.

The thickness of the calorimeter is clearly insufficient to attain a good energy resolution especially for the high energy hadrons expected at mountain altitudes. In addition, the sensitive area of $6 \times 6 \text{ m}^2$ is too small to cover the distribution of hadrons in the shower core completely. As far as the identification of single hadrons is concerned the same arguments apply as to the Akeno calorimeter. This part of the experiment appears to have been discontinued in the meantime. It has been replaced, since several years, by a much larger (162 m^2) X-ray emulsion chamber into which a few layers of ionization chamber have been incorporated [71]. The design of this chamber is similar to that of the Pamir experiment [72].

7.1.3 The EAS-TOP installation on Gran Sasso

The EAS-TOP installation [54] comprises an array of detectors for the electromagnetic component of extensive air showers and a calorimeter of $2 \times 135 \text{ m}^2$ which is intended for the measurement of hadrons above 50 GeV and of muons [73]. It is situated in the Gran Sasso mountains at an altitude of 2000 m on top of a large underground laboratory 1000 m below the array. The rate of sampling of the electromagnetic component is approximately a factor of two smaller than the corresponding figure of KASCADE.

Design and size of the hadron calorimeter are similar to ours. The total area is 270 m^2 (versus 320 m^2) and there are 10 active layers (versus 8). The total thickness of the KASCADE calorimeter is approximately 50 % larger which results in a better energy resolution for hadrons above 1 TeV. The spatial resolution of the EAS-TOP calorimeter is between 20 and 40 cm and therefore somewhat inferior. The main difference between the two designs lies in the choice of the active elements. The EAS-TOP design employs proportional counters which are very sensitive to changes in voltage, temperature, and ambient pressure and therefore much more difficult to operate under field conditions than the ionization chambers of the KASCADE design.

In addition to the hadron measurement the EAS-TOP calorimeter also allows for a very precise tracking of muons by use of a large number of streamer tubes which determine the position of single particles to a precision of 2 cm. It should be pointed out, though, that these detectors will also be sensitive to hadrons. It will therefore be hardly possible to identify muons in the shower core.

7.1.4 The ANI installation

This experiment is situated on top of Mt. Aragats (3250 m above sea level) in Armenia, USSR, where cosmic ray measurements have been performed for a long period of time. The original calorimeter of the installation employed 12 sensitive layers of ionization chambers between iron plates of 10 cm thickness shielded on top by two lead layers [74]. In each layer there is spatial resolution in only one direction. These are chosen mutually perpendicular in adjacent layers. The thickness of the calorimeter and the degree of longitudinal sampling guarantee a high energy resolution for single hadrons. The strip read-out employed for the ionization chambers makes the identification of individual hadrons very difficult, though, in the dense core of an air shower. The main disadvantage of the calorimeter is its limited size of 10 m². This is smaller than the usual size of the hadron distribution, therefore only part of the hadronic energy in the shower core can be registered.

Since several years a new and larger installation is under construction on Mt. Aragats [75] which will include a much larger hadron calorimeter of 1600 m². We have no detailed information on the design of the calorimeter nor on the present status of the new experiment.

7.2 Point source experiments

Following the discovery by the Kiel group [16] of excess cosmic rays from the direction of the well known astronomical object CYGNUS X-3 a large number of new extensive air shower experiments has been started and existing arrays have been modified to improve their angular resolution and/or sensitivity. A list of these experiments (taken mainly from the HEGRA proposal of the Kiel group) is given in table 7.1 and compared to our experiment although the investigation of point sources is not the main object of KASCADE. Of the experiments presently in operation or under construction CASA is clearly the largest. It will therefore be discussed in some detail in the next section.

7.2.1 The CASA experiment

This experiment [54] consists of an array of 1064 scintillation counters of 1.5 m² each on a total area of $2.5 \cdot 10^5$ m², i. e. 0.7 % of the array area are covered by detectors for the electromagnetic component of the showers. It is situated at the location of the famous Fly's Eye detector of the University of Utah at an elevation of 1460 m above sea level. A total of 1200 m² of scintillation counters for muons have been installed underground at the site. They can be operated in coincidence

both with the array and with the Fly's Eye. It is planned to double the muon detector area. Fast timing of the electron detectors ensures an angular resolution of better than 0.5° for primary energies above 3×10^{14} eV.

The large array area (twice the size of KASCADE) and the high angular resolution make CASA the most sensitive of all experiments presently in operation or under construction as far as the search of point sources is concerned. In addition, CASA has a very large detector area for muons and will therefore be able to measure the electron to muon ratio which is the observable most sensitive to the mass of the primary. It should be pointed out, though, that due to the simple design of the muon counters [76] it will probably not be possible to determine the number of muons hitting one of the 2.5 m^2 muon detectors. Hence the muon number in the shower core cannot be measured accurately and this may affect the precision to which the total muon number can be determined.

Measurements with the CASA array will start in early 1990 with half of the electron detectors installed. The complete system is expected to be finished by the end of 1990 [77].

7.2.2 Further point source experiments

Table 7.1 shows a list of extensive air shower experiments which aim at or can be used for the investigation of point sources. Since it is not always easy to obtain the latest information on the various installations we apologize for any omission or misinterpretation. The table does not include information on detector details or on the combination with other types of equipment such as air Cerenkov telescopes, calorimeters, or deep underground facilities. Quite a number of the entries represent older arrays which are now used for point source searches, some of them after having been modified to improve sensitivity and/or angular resolution. Experiments no more operational (such as the original Kiel experiment) have not been included. It is obvious from the table that KASCADE can compete with most of the installations as far as array and detector sizes are concerned. The same holds for the angular resolution. The main disadvantage of KASCADE is its low altitude which results in a rather high threshold (although the array at Kiel which yielded the original discovery was also situated near sea level). As discussed in section 4.8 above KASCADE will be able to make a substantial contribution also in this field if point source emission above 0.5 PeV turns out to exist.

Table 7.1: Extensive Air Shower Experiments Employed for the Search of Point Sources*

Name	Location	Latitude [°]	Longitude [°]	Altitude [m]	Size [m ²]			References
					Array	e.m.detectors	μ detectors	
Operational								
MSU	Moscow, USSR	55.7 N	37.4 E	192	$5 \cdot 10^5$	170	90	[78]
GREX	Haverah Park, UK	54 N	1.5 W	100	$3.5 \cdot 10^4$	36 x 1	40	[79]
BASA	Baksan, USSR	43.5 N	43 E	1700	$4 \cdot 10^3$	250	-	[80]
TIEN SHAN	Kirghizia, USSR	42.5 N	75 E	3340	$\sim 10^3$	~ 100	53	[81]
EAS-TOP	Gran Sasso, Italy	42.5 N	13.6 E	2000	10^5	29 x 10	270	[54]
DUGWAY	Utah, USA	40.5 N	112.3 W	1460	$4 \cdot 10^4$	33 x 1.5	8 x 158	[82]
BELJING	Huai Rou, China	40.4 N	116.7 E	~ 0	10^4	53 x 0.25	-	[85]
NORIKURA	Mt. Norikura, Japan	36.1 N	137.6 E	2770	$2 \cdot 10^3$	24 x 0.25	36	[83]
CYGNUS	Los Alamos, USA	35.9 N	106.7 W	2110	$2 \cdot 10^4$	108 x 0.83	44	[84]
SPICA	Akeno, Japan	35.5 N	138.5 E	900	$3 \cdot 10^4$	70 x 1	175	[86]
MT. HOPKINS	Arizona, USA	31.7 N	110.9 W	2350	10^3	13 x 1	-	[87]
HEGRA	La Palma, Can. Isl.	28.8 N	18.1 W	2200	$2.3 \cdot 10^4$	127 x 1	-	[25, 88]
MT. LIANG WANG	Kunming, China	24.8 N	102.9 E	2720	$2.8 \cdot 10^4$	37 x 0.25 + 3 x 1	3 x 17	[89]

Table 7.1 continued

Name	Location	Latitude [°]	Longitude [°]	Altitude [m]	Size [m ²]			References
					Array	e.m. detectors	μ detectors	
KGF	Kolar Gold Field, India	13 N	78.3 E	930	$7.5 \cdot 10^4$	127 x 1	7 x 29	[90]
OOTY	Ootacamund, India	11.4 N	76.8 E	2300	$5 \cdot 10^3$	24 (?)	-	[91]
SAS	Mt. Chacaltaya, Bolivia	16.3 S	68.1 W	5200	$8 \cdot 10^4$	16 x 1 +9 x 0.83	60	[92]
POTCHEFSTROOM	South Africa	26.5 S	27 E	1250	10^4	10 x 1	-	[93]
BUCKLAND PARK	Adelaide, Australia	35 S	138.5 E	~ 0	$3 \cdot 10^4$	19 x 1 +8 x 2.25	-	[94]
JANZOS	Black Birch Range, New Zealand	41.8 S	173.8 E	1640	$2 \cdot 10^4$	31 x 1 +45 x 0.5	-	[95]
SPACE	South Pole	90 S	-	2400	$6 \cdot 10^3$	16 x 1	-	[96]

Table 7.1 continued

Name	Location	Latitude [°]	Longitude [°]	Altitude [m]	Size [m ²]			References
					Array	e.m.detectors	μ detectors	
Under construction or planned								
KASCADE	Karlsruhe, Germany	49.1 N	8.4 E	110	$5 \cdot 10^4$	320 x 3	320 x 3 + 300	
GRAND	Notre Dame, USA	41.7 N	86.2 W	220	10^4	64 x 8	64 x 8	[97]
CASA	Dugway, Utah	40.5 N	112.3 W	1460	$2.5 \cdot 10^5$	1064 x 1.5	8 x 158	[98]
ANI	Mt. Aragats, Armenia	40.3 N	44.1 E	3250	$\sim 10^5$	60 x 1	1600	
LHASA	Tibet	30 N	91 E	4300	10^4	65 x 0.5	-	[99]
CRT	Mérida, Venezuela	8.6 N	70.9 W	3600	$3 \cdot 10^5$	385 x 2	385 x 2	[26]

General comments : Some relevant information on additional features such as atmospheric Cerenkov detectors, deep under ground facilities etc. are not included in the table. Also, the latest stage of development of the experiments may not always have been identified.

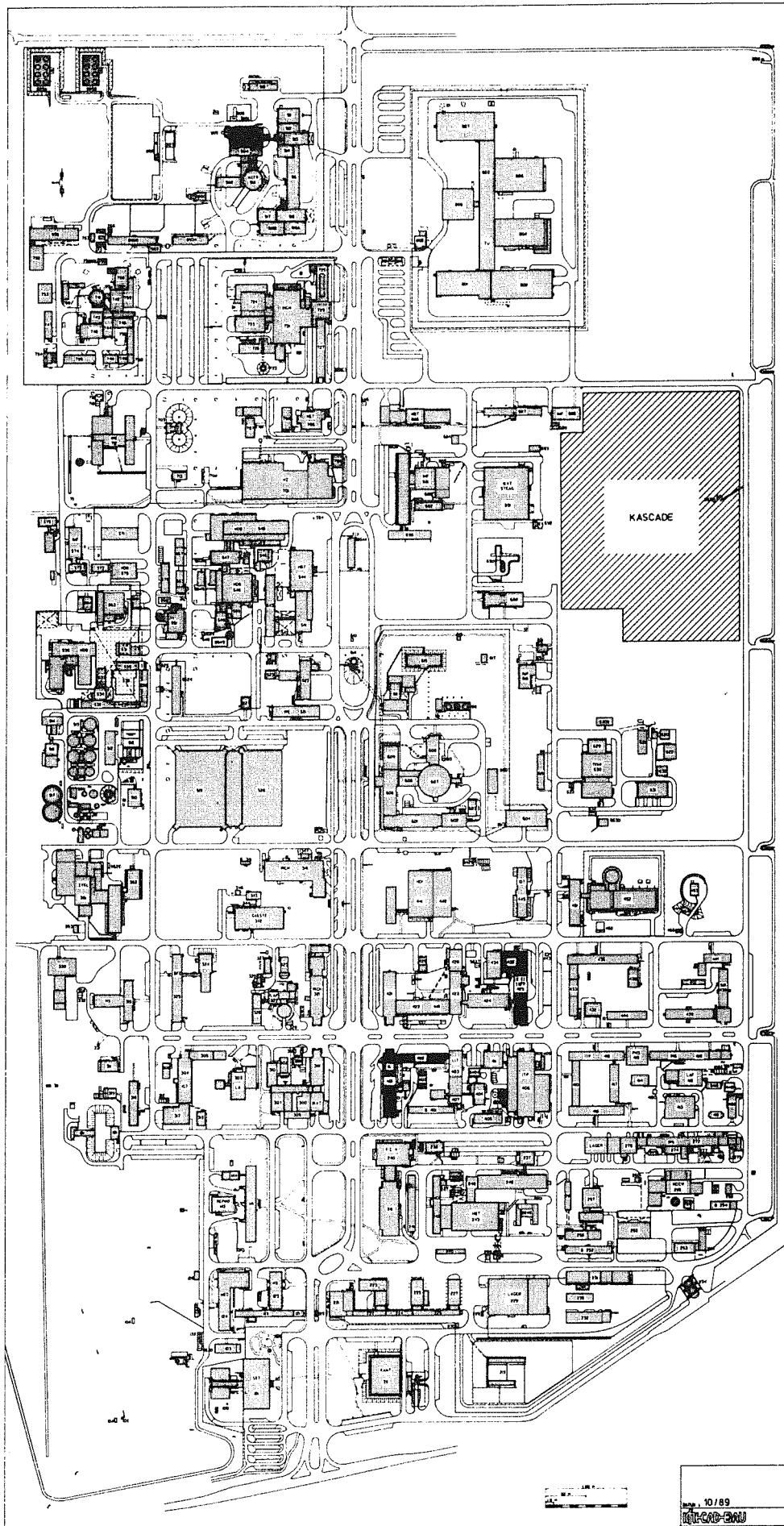


Fig. 8.1 Location of the KASCADE experiment

8. Concluding remarks

After an extensive discussion of various aspects a location of the KASCADE experiment within the area of Kernforschungszentrum Karlsruhe has been found suitable (fig. 8.1). Thus, the experiment will be embedded in the technical services of KfK. This will facilitate establishing the project in an optimum way. The detector system is modular so that measurements can be started relatively early and a later extension is possible.

The simulation of the air shower observables and of the detector response shows that the disadvantage of a location at sea level is compensated by a sufficiently large detection sampling and by more favourable economic conditions. We emphasize that the combined experimental study of electromagnetic, muonic, and hadronic components provides an important access to a more detailed insight into the nature of air showers.

The set-up of a prototype-cluster of array detectors is planned for early 1990 and followed by a continuous production of the field detectors. The clusters will be mounted during the years 1990 - 93. The basement of the central detector is expected to be completed in spring 1991 so that the iron stacking for the calorimeter can start in summer 1991. Casting the iron slabs has already started. The building of the central detector should be finished in 1992. The production of the ionization chambers (with an envisaged rate of 10 chambers per day), including test procedures, is planned to start in spring 1990.

We wish to thank all our colleagues who have discussed with us various experimental and theoretical aspects of the described project. In particular, we acknowledge the stimulating discussions and many valuable comments of J. Capdevielle, P. Grieder, A.M. Hillas, H. Lindenberger, D. Müller, G.B. Kristiansen, J. Trümper, A.A. Watson and J. Wdowczyk.

References

1. V.F. Hess, *Physikalische Zeitschrift* **13** (1912) 1084
2. P. Meyer, in: *Origin of Cosmic Rays*, IAU Symp. No. 94, G. Setti, G. Spada, and A. W. Wolfendale eds., Reidel 1981, p. 7ff
3. J. A. Simpson, *Ann. Rev. Nucl. Part. Sci.* **33** (1983) 323
4. J. P. Meyer, *Proc. 19th ICRC*, La Jolla 1985, **9**, 141
5. N. Lund, *Proc. 20th ICRC*, Moscow 1987, **8**, 45
6. J. M. Grunsfeld et al., *Astrophys. J.* **327** (1988) L31
7. D. Müller, private communication, 1988
8. W. I. Axford, in: *Origin of Cosmic Rays*, IAU Symp. 94, G. Setti, G. Spada, and A. W. Wolfendale eds., Reidel 1981, p. 339ff

9. H. J. Völk, Proc. 20th ICRC, Moscow 1987, 7, 157
10. P.O. Lagage and C. J. Cesarsky, Astron. Astrophys. 125 (1983) 249
11. H. J. Völk and P. L. Biermann, Astrophys. J. 333 (1988) L65
12. J. Linsley, Proc. 18th ICRC, Bangalore 1983, 12, 135
13. M. Samorski, private communication, 1989
14. M. Shima et al., Proc. 20th ICRC, Moscow 1987, 5, 240
15. K. G. Gibbs et al., Nucl. Instr. Meth. A264 (1988) 67
16. M. Samorski and W. Stamm, Astrophys. J. 268 (1983) L17
17. M. Samorski and W. Stamm, Proc. 18th ICRC, Bangalore 1983, 11, 244
18. P. G. Edwards et al., J. Phys. G: Nucl. Phys. 11 (1985) L101
19. J. Lloyd-Evans et al., Nature 305 (1983) 784
20. B. L. Dingus et al., Phys. Rev. Lett. 61 (1988) 1906
21. P. R. Vishwanath et al., Astrophys. J. 342 (1989) 489
22. L. Cassiday et al., Phys. Rev. Lett. 62 (1989) 383
23. M. A. Lawrence et al., Phys. Rev. Lett. 63 (1989) 1121
24. B. L. Dingus et al., Phys. Rev. Lett. 60 (1988) 1785; B. L. Dingus, Thesis, Univ. Maryland 1988
25. O. C. Allkofer et al., Proc. Workshop on Physics and Experimental Techniques of High Energy Neutrinos and VHE and UHE Gamma-Ray Particle Astrophysics, Arkansas 1989; Nucl. Phys. B in press
26. J. Heintze et al., Nucl. Instr. Meth. A277 (1989) 29
27. A. D. Serdyukov et al., Proc. 20th ICRC, Moscow 1987, 6, 356
28. G. B. Yodh, Proc. 20th ICRC, Moscow 1987, 8, 305
29. H. Sukuyama et al., Nuovo Cimento 4A (1983) 147
30. H. Sasaki et al., Proc. 20th ICRC, Moscow 1987, 6, 366
31. A. L. Hodson et al., Proc. 19th ICRC, La Jolla 1985, 7, 81
32. A. G. Ash, Proc. 19th ICRC, La Jolla 1985, 7, 94
33. P. V. Ramana Murthy and A. W. Wolfendale, Gamma-ray astronomy, Cambridge University Press 1986, chapt. 4
34. L. Scarsi et al., in: Origin of Cosmic Rays, IAU Symposium No. 94, G. Setti, G. Spada, and A. W. Wolfendale eds., Reidel 1981, p. 279ff
35. A. W. Wolfendale, *ibid.* p. 309ff
36. S. I. Nikolsky et al., J. Phys. G: Nucl. Phys. 13 (1987) 883
37. P. K. F. Grieder, Nuovo Cimento 84A (1984) 285
38. P. D. Acton et al., Proc. 20th ICRC, Moscow 1987, 6, 51
39. Ch. Geich-Gimbel, Int. J. Mod. Phys. A4 (1989) No. 4
40. J. N. Capdevielle, private communication, 1988
41. J. N. Capdevielle, J. Phys. G: Nucl. Phys. 15 (1989) 909

42. A. Klar and J. Hüfner, Phys. Rev. **D31** (1985) 491
43. J. Hüfner et al., Phys. Lett. **166B** (1986) 31
44. C. J. Batty et al., Adv. Nucl. Phys. **19** (1989) 1
45. H. de Vries et al., Atom. Data Nucl. Data Tables **36** (1987) 495
46. P. K. F. Grieder, Abbreviated Description of SH2C-60-K-OSL-E-SPEC Shower Simulation Program and Model Options, unpublished report, Physik. Inst. Universität Bern (1980); private communication (1988)
47. P. K. F. Grieder, Proc. 15th ICRC, Plovdiv 1977, **8**, 370
48. K. Greisen, Progr. Cosmic Ray Phys. **3** (1956) 1
49. A. M. Hillas, Proc. 17th ICRC, Paris 1981, **6**, 244
50. W. R. Nelson et al., The EGS4 Code System, Stanford Report SLAC-265 (1985)
51. R. M. Sternheimer et al., Phys. Rev. **B26** (1982) 6067
52. J. Spitzer, private communication (1988)
53. GEANT : CERN report DD / EE / 84 / 1 (1987)
54. CASA : K.G. Gibbs et al., Nucl. Instr. Meth. **A264** (1988) 67
HEGRA : W. Stamm, Workshop Bad Liebenzell, Mai 1988
Gran Sasso : M. Aglietta et al., Nuovo Cim. **9C** (1986) 262,
M. Aglietta et al., Nucl. Instr. Meth. **A277** (1989) 23
CYGNUS : B.L. Dingus et al., Phys. Rev. Lett. **60** (1988) 1785
55. E. Iarocci, Nucl. Instr. Meth. **217** (1983) 30
56. M. Samorski, W. Stamm, APJ **268** (1983) L17
57. J.-M. Bonnet-Bidaud, G. Chardin, Phys. Reports **170** (1988) 327
58. J. Engler, internal reports, Kernforschungszentrum Karlsruhe, unpublished
59. J. Engler and H. Keim, Nucl. Instr. and Meth. **223** (1984) 47
J. Engler, H. Keim and B. Wild, Nucl. Instr. and Meth. **A252** (1986) 29
J. Engler, H. Keim and C. Müller, Nucl. Instr. and Meth. **A254** (1987) 311
60. R. Aleksan et al., Nucl. Instr. and Meth. **185** (1981) 95
61. J. Knapp, internal report, Kernforschungszentrum Karlsruhe, unpublished
62. C. Rubbia, private communication
63. R.P. Kokoulin and A.A. Petrukhin, Nucl. Instt. and Meth. **A263** (1988) 468
64. T. Hara et al., Proc. 16th ICRC, Kyoto 1979, **8**, 135; K. Kamata et al., Proc. Conf. Cosmic Rays and Particle Physics 1978, T. K. Gaisser ed., AIP Conf. Proc. no. 49 (1979) 443
65. M. Teshima et al., Nucl. Instr. Meth. **A247** (1986) 399
66. S. Kawaguchi et al., Proc. 21st ICRC, Adelaide 1990, **4**, 294
67. M. Nagano et al., J. Phys. G: Nucl. Phys. **10** (1984) 1295; M. Teshima et al., J. Phys. G: Nucl. Phys. **12** (1986) 129

68. T. Hara et al., Proc. 20th ICRC, Moscow 1987, 5, 477
69. D. S. Adamov et al., Proc. 20th ICRC, Moscow 1987, 5, 460
70. T. P. Amineva et al., Trudy FIAN 46 (1970) 157
71. S. F. Abdrashitov et al., Izvest. Akad. Nauk SSR, Ser. Fiz. 50 (1986) 2203
72. S. G. Baiburina et al., Trudy FIAN 154 (1984) 6
73. M. Aglietta et al., Proc. 21st ICRC, Adelaide 1990, 10, 316
74. V. V. Avakhian et al., Izvest. Akad. Nauk, Ser. Fiz. 49 (1985) 1315
75. CERN Courier, March 1987, p. 15; A. P. Garyaka and E. A. Mamidjanian, Proc. 5th Internat. Symp. Very High Energy Cosmic Ray Interactions, M. Giler ed., contrib. papers, p. 336
76. D. Sinclair, Nucl. Instr. Meth. A278 (1989) 583
77. D. Müller, private communication (1990)
78. S.N. Vernov et al., Izvest. Akad. Nauk SSSR, Ser. Fiz. 44 (1980) 537; G.B. Khristiansen, private communication (1989)
79. S.D. Bloomer et al., Proc. 21st ICRC, Adelaide 1990, 4, 314
80. V.V. Alexeenko et al., Proc. 21st ICRC, Adelaide 1990, 4, 302
81. S.F. Abdrashitov et al., Izvest. Akad. Nauk SSSR, Ser. Fiz. 50 (1986) 2203; W.S. Azeikin et al., Trudy FIAN 109, (1979) 3
82. G.L. Cassiday et al., Proc. 21st ICRC, Adelaide 1990, 9, 94
83. M. Amenomori et al., Proc. 21st ICRC, Adelaide 1990, 2, 27; K. Nagashina et al., Nuovo Cim 12C (1989) 695
84. D. Berley et al., Proc. 21st ICRC, Adelaide 1990, 10, 301
85. Y.H. Tan et al., Proc. 21st ICRC, Adelaide 1990, 10, 286
86. P.G. Edwards et al., Proc. 21st ICRC, Adelaide 1990, 4, 298
87. G.H. Gillander et al., Very High Energy Gamma Ray Astronomy, K.E. Turrer ed., Reidel 1987, p. 261
88. V. Hausteijn et al., HEGRA-Proposal, unpublished 1989
89. L.K. Ng et al. Proc. 21st ICRC, Adelaide 1990, 4, 286
90. S. Sinha et al., Proc. 21st ICRC, Adelaide 1990, 4, 334
91. A.R. Apte et al., Proc. 19th ICRC, La Jolla 1985, 3, 469
92. R. Kaneko et al., Proc. 20th ICRC, Moscow 1987, 2, 431
93. E.J. de Villiers et al., J. Phys. G: Nucl. Phys. 12 (1986) 547
94. P.C. Crouch et al., Nucl. Instr. Meth. 179 (1981) 467; D.J. Bird, private communication (1990)
95. I.A. Bond et al., Phys. Rev. Lett. 60 (1988) 1110
96. N.J.T. Smith et al., Nucl. Instr. Meth. A276 (1989) 622
97. J. Poirier et al., Proc. 20th ICRC, Moscow 1987, 2, 438

98. K.G. Gibbs et al., Proc. 21st ICRC, Adelaide 1990, 4, 306;
B.J. Newport et al., Proc. 21st ICRC, Adelaide 1990, 4, 310
99. A.X. Huo, Proc. 21st ICRC, Adelaide 1990, 2, 427
100. E.V. Danilova et al., Proc. 18th ICRC, Bangalore 1983, 5, 527